4.4 Nanoscale: Mineral Weathering Boundary

RI Dorn, Arizona State University, Tempe, AZ, USA
SJ Gordon, United States Air Force Academy, Colorado Springs, CO, USA
D Krinsley and K Langworthy, University of Oregon, Eugene, OR, USA

Glossary

Back-scattered electron (BSE) microscopy An accelerated electron beam in an electron microscope produces collisions between electrons and atoms, where the largest atoms with the higher atomic number (Z) generate a brighter intensity when imaged with a back-scattered detector.

Biotic weathering Mineral weathering caused by life, including bacteria, fungi, algae, plants, and animals.

Case hardening The outer shell of a rock that has been hardened (indurated) through the addition of elements such as silica or iron.

Etching of minerals Mineral dissolution is not an even produce; areas of more intense dissolution are seen as pits on the scale of micrometers.

Heavy metal scavenging Iron and manganese oxides and hydroxides scavenge heavy metals such as zinc, copper, and lead.

High-resolution transmission electron microscopy (HRTEM) Two-dimensional spatial imaging of very thin samples able to image mineral lattices with a spatial resolution of >0.08 nm.

Microfractures Breaks in minerals that can carry capillary water.

Nanoscale Features between 1 nm (10^{-9} m) and 100 nm (10^{-7} m) or 0.1 μm.

Splintering Rock fracturing in a pattern of subparallel fractures that resembles a book that has been thrown in water and then dried.

Thermal fracturing Breaking of minerals from the process of heating and cooling, such as the passage of a wildfire over rock surfaces.

Abstract

This chapter presents the first overview of the connection between nanoscale weathering and geomorphology, where three overarching themes recur. First, nanoscale processes are on one side of a fundamental threshold between the coarser microscale (micrometers and up) and the finer nanoscale with its dramatically different molecular dynamics. Second, nanoscale processes do impact a variety of prior geomorphic research, including threads related to ongoing instability in mineral weathering, silt production, rock coating behavior, geochemical pollution, thermal weathering from wildfires, and biotic weathering as an explanation for deviations from Goldich's weathering series. Third, it is possible to link the nanoscale to more classic geomorphic concerns through scaling up quantitatively by digital image processing of microscope imagery and conceptually through connections to weathering forms such as rock splintering.

4.4.1 Introduction to Nanoscale Weathering

Scale is a vitally important concern in the development of geomorphic weathering theory (Phillips, 2000; Viles, 2001; Turkington et al., 2005; Hall, 2006a, 2006b). Scale is a key variable in the boundary layer model designed to interpret spatial variability in weathering (Pope et al., 1995). Scale issues have consumed much thought and research trying to link the largely disparate weathering subfields of controlled laboratory studies and field-based investigations (Brantley and Velbel, 1993; Casey et al., 1993; Swoboda-Colberg and Drever, 1993; Banfield and Barker, 1994; Brantley and Mellott, 2000; Brantley, 2005; Turkington and Paradise, 2005; White, 2005; Zhu et al., 2006; Meunier et al., 2007; Navarre-Sitchler and Brantley, 2007). The solution to the discrepancy between field and laboratory studies may rest in weathering interactions with nanoscale particles (Emmanuel et al., 2010; Emmanuel and Ague, 2011).

Thresholds are also an important focus in geomorphic weathering research (Paradise, 1995; Pope et al., 2002). A key scale threshold exists between nanoscale processes and those operating even at the micron scale. In his 2001 presidential address to the Geochemical Society, Michael Hocehlla, Jr. emphasized:

> nanoscience is based on the premise that materials properties in the bulk do not simply scale into the nanodomain, but property modification, and in some cases entirely different properties, are to be expected … In the nanoscale size range, physical, electrical, magnetic, thermal, kinetic, and other properties can be altered dramatically simply due to the physical dimensions of the material. (Hochella, 2002b: 738).

Interactions at the micron scale simply do not reflect molecular dynamics in the nanoscale chemical environment, in part because processes at the nanoscale can undergo substantial changes when exposed to water (Zhang et al., 2003; Wang et al., 2006; Kalinichev et al., 2007; Baram et al., 2011). Wang et al. (2006: 579) summarize the findings of a molecular modeling approach:

> The atomic density profiles of water perpendicular to the surface are largely controlled by the mineral surface structure. The orientations of these molecules, however, are dominantly influenced by surface hydrophobicity, surface charge distribution, and the ability to form H-bonds with adsorbed water molecules. The first molecular layers of water at all the surfaces are well ordered parallel to the surface, reflecting the substrate crystal structure and composition. This structure, however, is different from that of ice. The mobility of adsorbed water molecules and the enthalpy of surface hydration are controlled by mineral surface charge and hydrophobicity.

Nanoscale is typically defined as examining features between 1 nm (10^{-9} m) and 100 nm (10^{-7} m) or 0.1 μm (Figure 1). One way to visualize the nanoscale is to look at your hand; the scale difference between the entire Earth and your hand is the same dimensional scale difference as your hand and a nanoparticle. Nanoscale processes are not included in the microscale, defined by Pope et al. (1995: 220) as being sub-millimeter, because a very different realm of weathering processes operate below 0.1 μm. Research on nanoscale weathering is still in its infancy, having grown up with progressive improvements in high-resolution transmission electron

microscopy (HRTEM) since the 1980s. The first of this research tended to focus on the very different water–mineral interaction that occurs in the nanodomain within minerals, in that even microfracture capillary water (Meunier et al., 2007) behaves differently from water held within mineral internal surfaces (Hochella, 2002b). The first decade in the twenty-first century has seen a diversification of nanoscale weathering research, including the beginnings of attention paid to connections between geomorphology and nanoscale processes.

This chapter focuses on case studies of nanoscale weathering from a geomorphic perspective. Nanoweathering alters minerals and also produces nanoparticles through mechanisms such as chemical weathering, abiotic precipitation, and microbial processes. Although geomorphic research on spatial variability in nanoscale weathering is in its infancy, nanoparticles do have spatially specific point sources. They can derive from human pollution. They can be the result of anthropogenic alterations of a biogeochemical environment. Spatially explicit geochemical pathways alter geochemical cycles in soils, in phreatic water, and in rivers. Exactly how the study of nanoscale weathering will alter the field of geomorphology is not possible to predict at this point. Not enough research has been carried out at the nanoscale to understand links to landforms. Thus, a primary goal of this chapter simply rests in opening a dialog between the nanoscale and the landform scale through case studies of nanoscale weathering in different geomorphic contexts.

4.4.2 Nanoscale Techniques for Geomorphologists

4.4.2.1 Nanoscale Resolution Electron Microscopy

The study of earth materials has been enhanced in the past decade through the use of HRTEM and other high precision techniques. Ongoing technique developments over the past three decades have led to an array of imaging and analysis tools available to examine weathering processes and products (Table 1). Each technique has its advantages and limitations that are reviewed in detail elsewhere (Lee, 2010). This section overviews a few options that could be used in geomorphological studies of nanoscale weathering.

The basic idea behind high-resolution microscopy is to thin a sample enough so that electrons can pass through the sample upon irradiation with a 80–300 kV electron beam. Given the nature of the material and the particular techniques used, the thickness for high-resolution imaging can vary from ∼ 10 to 50 nm. Today, most HRTEM specimens are prepared using a coupled dual-beam focused ion beam electron microscopy (FIB-EM). The FIB-EM can site specifically ion mill and deposit metals; coupled with a micromanipulator, the FIB-EM can extract features/regions on the order of 10–30 μm wide and carry out nanoscale tomography (Schiffbauer and Xiao, 2009). Once extracted and mounted to a transmission electron microscopy (TEM) grid *in situ*, the FIB-EM is used to thin the extracted region until it becomes electron transparent and usable in the TEM (generally referred to as a 'lamella') (Brown and Lee, 2007). FIB-EM-prepared samples have many advantages, such as allowing investigators to see the context of a lamella in back-scattered electron detector (BSE), secondary
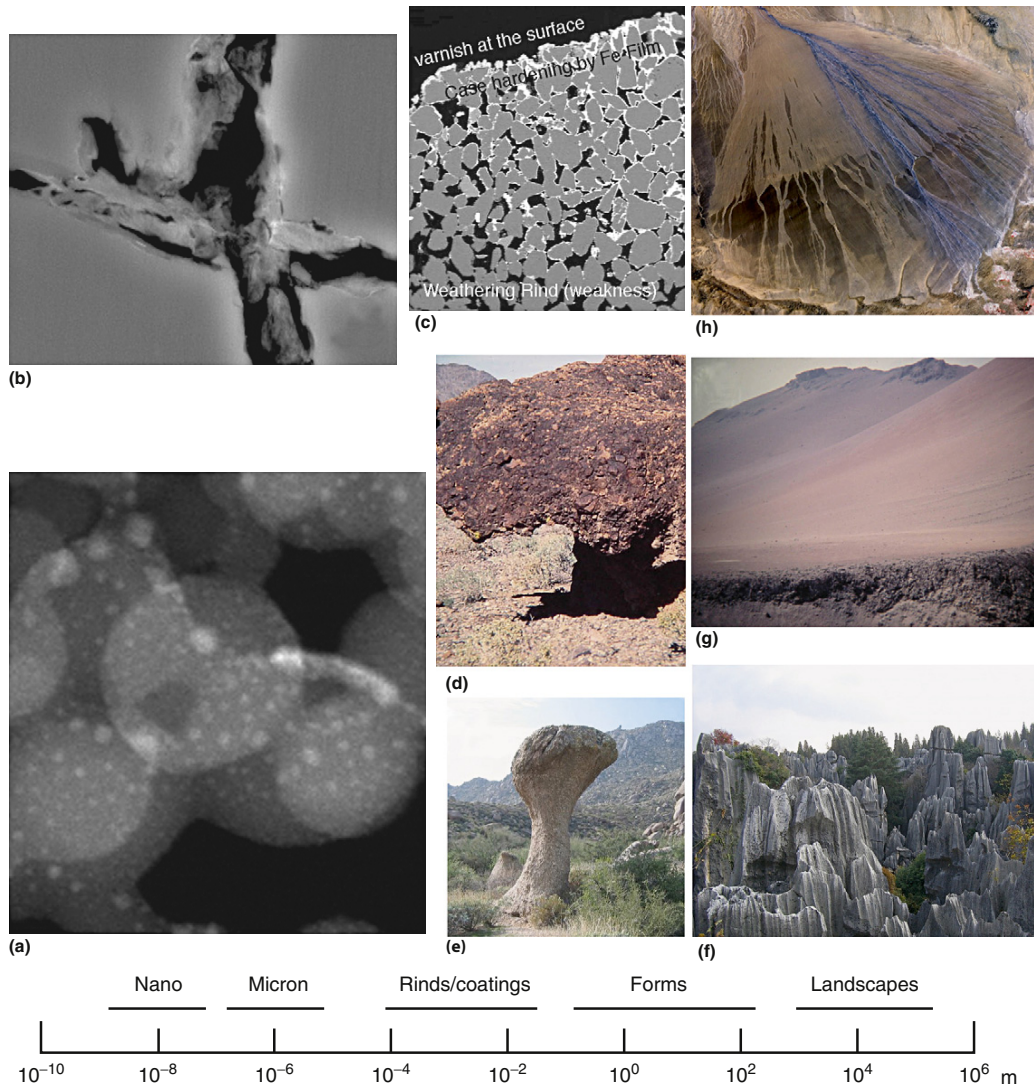
Figure 1 Visualization of nanoscale weathering placed within broader spatial scales of weathering phenomenon. Examples presented from nano to landscape scales are: (a) nanoscale silica spheoids a few tens of nm across from silica glaze in Tibet (high-resolution transmission electron microscopy (HRTEM) image); (b) micron-scale silt formation from quartz weathering in Arizona (back-scattered electron (BSE) image); (c) millimeter to centimeter-scale rock coatings and weathering rinds illustrated from Wyoming (BSE image) and (d) Death Valley (case hardened rock shelter); (e) meter-scale weathering forms of a mushroom rock, Arizona and (f) limestone karst stone forest, Kunming, China; and (g) kilometer-scale weathering landscapes of a salt-encrusted marine terrace, Peru, and (h) varnish-coated alluvial fan, western China, courtesy of NASA.

electron (SE), scanning/transmission electron microscopy (STEM), and energy dispersive X-ray spectroscopy (EDS) modes prior to breaking vacuum and moving the specimen to a TEM for higher-resolution analysis. Other techniques used to prepare samples for TEM include mechanical crushing of minerals, which can generate edges that are sufficiently electron transparent, and ultramicrotoming, which can prepare electron transparent slices of material using a diamond knife. Tripod polishing and precision ion polishing (PIPS) are also useful for obtaining electron transparent areas from bulk specimens for TEM analysis.

Use of TEMs/STEMs begins with placement of the TEM grid into a sample holder and insertion of the holder through an airlock into a high vacuum electron column. HRTEMs use much higher electron beam voltages (typically from 80 to 300 kV) than scanning electron microscopies (SEMs). The high voltage, coupled with a thin sample, decreases interaction volume and allows EDS measurements to be made with spot sizes of < 10 nm, in contrast to typical SEM interaction volumes on the order of $\sim 1 \, \mu m$ at 15 kV with thicker/bulk samples. Many times the spot size can be seen as beam damage on thin samples, leaving behind a series of holes or

Table 1   Overview of nanoscale microscopy techniques useful in weathering research

Technique (and acronym)	Information obtained	Spatial resolution	Limitations
Coupled dual-beam focused ion beam electron microscopy (FIB-EM)	Used to create and image cross-sections *in situ*, widely used to extract sections for TEM analysis. Real time imaging in SEM mode during ion milling.	$> \sim 1$ nm	Maximum sample and scan size, requires vacuum, Ga ion implantation.
High-resolution transmission electron microscopy (HRTEM)	2-D spatial imaging, lattice imaging.	>0.08 nm	Small area, sample preparation challenges, sample thickness <50 nm.
Energy dispersive X-ray analysis (EDS)	Elemental composition, X-ray mapping of elements.	>1 nm (HRTEM); >20 nm (SEM)	Detection limit varies, ~ 0.2 wt.%. Difficult for light element detection.
Energy-filtered TEM (EFTEM)	Mapping of elements detectable from EELS spectrum.	<1 nm	Best results with light elements, requires high vacuum and thin specimens.
Scanning transmission electron microscopy (STEM)	2-D special imaging, high contrast.	<1 nm	Requires vacuum, thin specimen.
Scanning electron microscopy (SEM) with back-scattered electron detector (BSE)	Average atomic number (Z) revealed through contrast I grayscale image.	>5 nm	Generally requires vacuum (dry samples), sample size dependent on chamber size.
Scanning electron microscopy (SEM) with secondary electrons (SEs)	2-D spatial imaging.	>1 nm	Requires vacuum, sample size dependent on chamber size
Atomic force microscopy (AFM or FM)	3-D surface microtopography.	<1 nm in Z, <10 nm X,Y	Maximum scanning area of about 150×150 microns. Flat samples ideal.
Secondary ion mass spectroscopy (SIMS)	Elemental and isotopic composition.	50 nm with NanoSIMS	Requires vacuum, damages analysis region.

grid patterns (e.g., Lee, 2010: 10). The high spatial resolution of STEM and the ability to utilize atomic number (Z) contrast makes it a particularly powerful tool in weathering studies (Brown and Lee, 2007).

Nanoscale studies of weathering samples generate a variety of different types of imagery formed by filtering scattered electrons. Bright-field images are generated from a direct beam that contains unscattered and low-angle forward scattered electrons. Dark-field images, by contrast, are generated only from forward-scattered electrons. The thickness, atomic number, and Bragg diffraction (in crystalline material) will control the angle of scattering and the intensity of scattering – all creating the HRTEM image. Since mineralogy is characteristically important in weathering, electron diffraction patterns record the angular distribution of electrons where minerals can be identified by the spacing of spots using selected-area electron diffraction (SED), precession electron diffraction (PED), or convergent-beam electron diffraction (CBED). It is also possible to generate images of specific elements at the subnanoscale using energy-filtered TEM imaging that takes a specific region of an electron energy loss spectroscopy (EELS) spectrum to form an image.

Compositional analysis is typically carried out by EDS for higher atomic number elements and EELS for lighter elements. EELS measures energy lost through ionization of sample atoms, separating electrons according to the energy they have lost. EELS can measure elemental abundance and also determine valence states at spatial resolutions less than 1 nm.

4.4.2.2   Linking Scales through Digital Image Processing

An increasingly important weathering literature focuses on explaining offsets between field-based quantification of weathering and laboratory studies of weathering rates (Brantley and Velbel, 1993; Casey et al., 1993; Swoboda-Colberg and Drever, 1993; Banfield and Barker, 1994; Brantley and Mellott, 2000; Brantley, 2005; Turkington and Paradise, 2005; White, 2005; Zhu et al., 2006; Meunier et al., 2007; Navarre-Sitchler and Brantley, 2007; Emmanuel et al., 2010; Emmanuel and Ague, 2011). Brantley (2005: 108) concisely summarized some key issues:

> … extrapolating from one scale to another (scaling up) is often not quantitatively successful. For example, quantitative extrapolation of laboratory rates to field systems remains difficult, and we now recognize that multiple factors contribute to this discrepancy. For example, intrinsic factors related to differences in mineral samples prepared in the laboratory or weathered in the field contribute to the laboratory-field discrepancy. Of particular importance is the reactive surface area of dissolving minerals: this term must be investigated and understood more thoroughly. In addition, laboratory rates are generally measured far from equilibrium, whereas natural weathering often occurs closer to equilibrium where dissolution is slower. This difference in chemical affinity is a consequence of the hydrological complexity of natural systems wherein fluids at mineral interfaces may approach equilibrium. Thus, dissolution of laboratory samples may generally be rate-limited by the interface reaction while dissolution in field systems may at times become partially rate-limited by transport. The scaling-up problem inherent in the laboratory-field discrepancy may well be solved through increased understanding developed as we bridge scales of analysis from the nano to global scale…
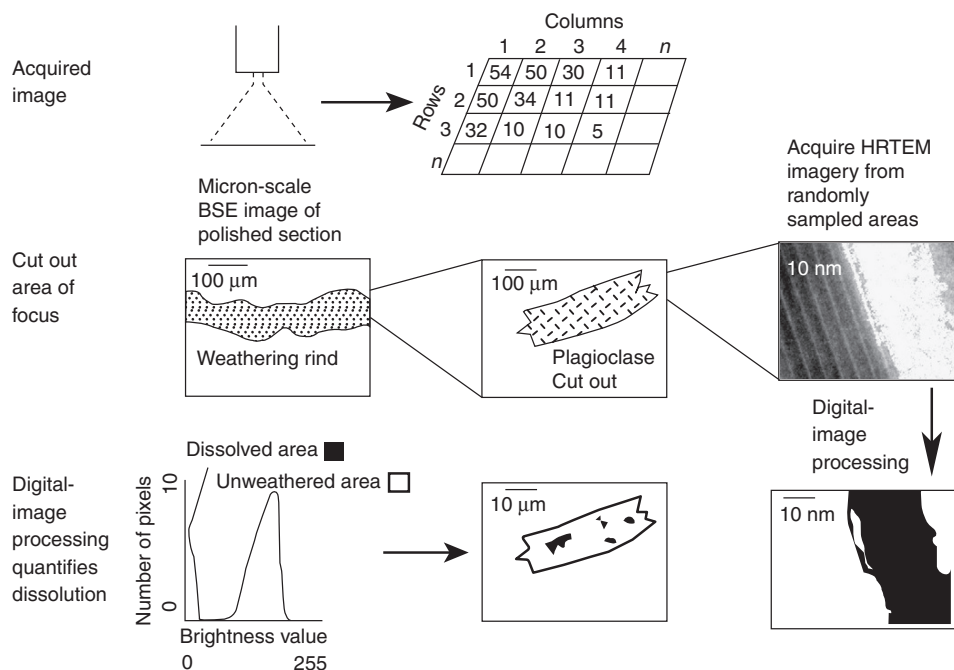
Figure 2   Connecting field and lab results, as well as rescaling weathering rates is feasible using digital-image processing of dissolved minerals. Originally developed for measuring weathering rates over thousands of years in field samples at the micron scale with BSE imagery, this approach can also directly compare laboratory with field samples and the same samples at scales ranging from square nanometers to square millimeters.

Meunier et al. (2007: 432) explicitly advocates that the missing link in bridging scales rests at the scale of hand specimens:

> As weathering is a multi-scale phenomenon, theoretically any model needs to integrate the solid-fluid exchanges from the atomic interactions at the very surface of primary and secondary minerals (nanometre), to the rock sample (decimetre) and finally to the watershed (kilometre). However, such integration is currently beyond our calculation abilities. Hence we have to focus on the strategic aspect of weathering processes, although deciding where and on which variables to focus our attention remains difficult. It is remarkable that our understanding of the physicochemical weathering processes is much more advanced at the extreme scales of nanometres to tens/hundreds of kilometres, that at intermediate scales. At the nanometre level, the experimental and theoretical studies cover the observation of natural samples. The extensive use of high-resolution transmission electron microscopy (HRTEM), atomic force microscopy (AFM) and spectroscopy have significantly improved our knowledge of fluid-mineral reactions and their related interactions. Conversely, the large-scale studies based on isotope mass balance methods provide denudation rates for provinces or continents. Surprisingly, it is at the hand-specimen scale where efforts should now be directed.

One strategy that could help bridge the discrepancy at the hand-sample level is *in situ* quantitative analysis of mineral dissolution (Dorn, 1995) using digital image processing (e.g., Figure 2). This direct measurement of mineral dissolution has led to an understanding of field relationships on the temperature dependence of weathering (Dorn and Brady, 1995), and understanding of the effects of rainfall and temperature on mineral weathering (Brady et al., 1999), long-term rates of glass dissolution (Gordon and Brady, 2002), and the role of

lichens and rock coatings on field mineral weathering rates (Gordon and Dorn, 2005a, 2005b).

Although digital image processing of BSE imagery has only been used to analyze field weathering that has taken place over 10^1–10^5 years and at the micron scale, there is no reason why laboratory samples or nanoscale samples could not be similarly analyzed. For example, the subnanometer conduits that carry aqueous fluids (Banfield and Barker, 1994) or the nanoscale etch pits could be prepared for digital image processing to quantify nanoscale porosity (Figure 2).

Previous research on digital image processing to quantify weathering has focused on the micron scale, typically measuring 10^5 μm^2 of mineral cross sections imaged with BSE per field site. New advances in electron microscopy have increased the resolution of back-scatter images. It is now possible to analyze mineral dissolution at the nanoscale with BSE (e.g., Figure 3). Scaling up (cf. Brantley, 2005: 108) and then scaling down becomes a task of taking lower-resolution BSE and higher-resolution BSE images using STEM at different scales and measuring *in situ* dissolution. Measurement of field and laboratory-weathered samples alike at different scales, thus, enables the integration of data to the hand-sample level – as advocated by Meunier et al. (2007).

4.4.3   Applying Nanoscale Strategies to Contemporary Issues in Geomorphic Weathering

The goal of this section rests in highlighting different areas of research in geomorphology where attention to the nanoscale
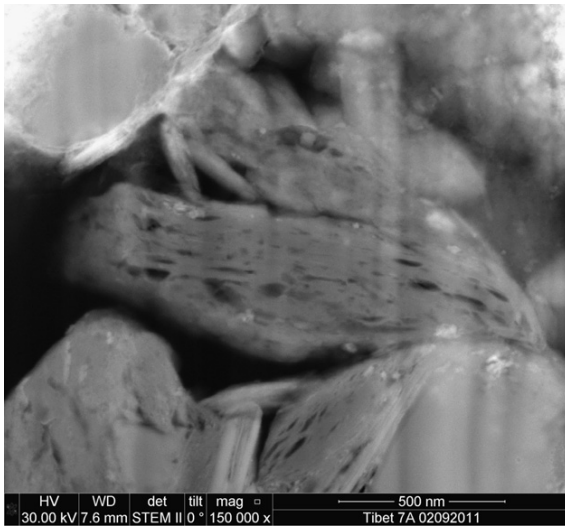
Figure 3 High-resolution STEM image in dark field mode, which provides contrast similar to BSE. The dust particles, resting on a rock coating from the Akesu Volcanic Field, were lifted out, thinned using the ion beam, and then mounted perpendicular to the beam to allow electrons to transmit through the sample onto a STEM detector. Prior to digital-image processing, each mineral would be cut out separately and made into its own image. Then, the void spaces would be made its own image and counted digitally given an area of the mineral that has dissolved (cf. Dorn, 1995).

has either yielded new insights or has the potential to generate new theory about weathering. This section starts by illustrating the potential of nanoscale research in studies of biotic weathering. The second case study presents a cautionary tale of where a lack of attention to the nanoscale/micron-scale threshold has created problems in interpretation. The other case studies explore different facets of weathering including etching, dust weathering, case hardening, thermal weathering, silica glaze formation on Mars, and the importance of nanoscale processes in understanding lead contamination of rock surfaces.

4.4.3.1 Biotic Weathering

Research on biotic weathering is taking on increasing importance with the general observation that bacteria and other microorganisms occur at great depth in the Earth (Reith, 2011). Biotic weathering occurs at the micron scale and the nanoscale. This section exemplifies research at both scales, starting with the micron scale and a classic mystery in the field of weathering surrounding weathering of olivine, one of the first minerals to crystallize as a magma cools. Then, this section moves into the nanoscale where the higher resolution provides new insights on how microorganisms play a vital role in mineral weathering.

The generally accepted view has been that mineral weathering is the reverse of Bowen's reaction series that explains mineral crystallization. The weathering sequence published by Goldich (1938) is the opposite of Bowen's sequence. It starts erroneously with the notion of the weathering of olivine, since olivine formed at the hottest temperatures, and ends with quartz being one of the most stable minerals, because it formed last at the coolest temperatures.

A flaw in this thermodynamic interpretation was discovered through field-based research using BSE to study the surfaces of lava flows of Hualalai, Hawaii. This research revealed that olivine does not weather first (Wasklewicz et al., 1993; Wasklewicz, 1994), as predicted by the Goldich weathering sequence (Goldich, 1938). The field sites where olivine weathered last, not first, had a paucity of organic acids – being located in the rainshadow of both Mauna Loa and Hualalai. Olivine was much less weathered than plagioclase and clinopyroxenes in those lava-flow surfaces devoid of acid-producing lichens and fungi and distant from vegetation. By contrast, olivine weathered much faster at lava-flow surfaces that hosted acid-producing organisms. Nanoscale research may hold the key to explain the apparent contradiction between Goldich's (1938) sequence and the observations from the rainshadow of Hawaii.

Goldich's (1938) original field sites were located in a humid environment that contained abundant organic acids and organisms. Other workers have confirmed Goldich's sequence in similar humid environmental settings (Velbel, 1993). A working hypothesis is that Goldich's weathering sequence could be more a function of biotic weathering environment than the thermodynamics of mineral formation. Furthermore, olivine has a lower elemental bond strength than quartz.

An important biotic influence on the sequence of mineral weathering could be microbial weathering. Laboratory research on bacterial weathering at the micron scale determined that Goldich's weathering sequence is in accord with the vulnerability of minerals to bacteria (Song et al., 2010). **Figure 4** illustrates some of the evidence presented by Song et al. (2010) in their controlled laboratory experiment, illustrating how bacteria can promote dissolution of plagioclase through pitting. One possible reason for microbial activity causing the Goldich sequence could be the nutrient needs of microbes (Bennett et al., 2001):

> A basic tenet of sediment diagenesis, the "Goldich Weathering Sequence" (Goldich, 1938), states that the most unstable silicate mineral will weather (dissolve) first, with more resistant silicates taking progressively longer to dissolve (from least to most stable), olivine < plagioclase < albite < anorthoclase < microcline < quartz. The observed weathering sequence of minerals in an anaerobic, microbially controlled system, however, is almost opposite, with olivine stable with respect to microcline, and the relationship between microbial colonization and weathering rate almost perfectly correlated. This suggests that, in some environments, the indigenous microorganisms may significantly alter weathering patterns as they aggressively scavenge limiting nutrients. (Bennett et al., 2001: 16)

One possible nanoscale explanation for the discrepancy between Goldich's sequence and weathering in abiotic contexts (Barker and Banfield, 1996: 55) follows:

> Biologically mediated weathering involves a complex dissolution/selective transport/recrystallization mechanism occurring within the acidic extracellular gels coating all mineral surfaces. A specialized weathering microenvironment around each mineral grain initially produces minute phyllosilicate crystallites. A rind of clay minerals forms around the dissolving parent phase, eventually culminating in abundant 5–10 μm diameter polymer-bound aggregates of face-to-face oriented clay minerals of homogeneous composition. Physiochemical weathering of ferrohastingsite produces topotactically oriented smectite and goethite. The cleavage-controlled reaction is neither isochemical nor isovolumetric.
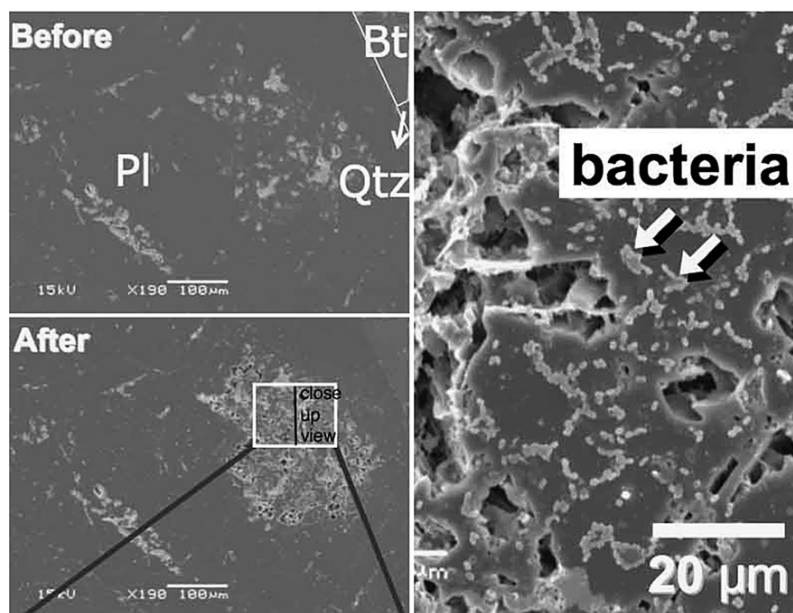
Figure 4 A granite cross-section viewed in secondary electrons before and after being subject to bacterial weathering. An extensive microscope study analyzed weathering in the laboratory abiotically and biotically. This type of micron-scale controlled laboratory study is an ideal precursor to a nanoscale investigation of exactly how bacteria generate increased pitting. We thank Dr. Wonsuh Song of the University of Tsukuba for permission to use these micrographs.

A sub-40-nm scale study of microbial weathering of a Mg–Fe–pyroxene in a meteorite that was exposed to weathering for about 70 years (Benzerara et al., 2005a, 2005b) provides additional insight. Microbial interactions over seven decades led to carbonate precipitation in the form of rod-shaped nanocrystals of calcite and the development of an amorphous Al-rich layer – all leading to the conclusion that microorganisms create nanoscale weathering environments that dramatically alter weathering. Micron- and nanoscale studies of fungal and bacterial weathering of an exposed granitic pegmatite similarly stress the importance of microbial ecology in subaerial settings (Gleeson et al., 2005, 2006).

One possible way that microorganisms might affect weathering is through interactions with fungal hyphae. Nanoscale *in situ* observations of a soil fungus interacting with biotite over 3 months revealed a nanoscale attachment to the mineral. Biomechanical forcing altered interlayer spacings, and microbial processes leached potassium, all leading to the formation of vermiculite and clusters of oxidized iron (Bonneville et al., 2009; Smits et al., 2009). These clusters of iron oxides are features commonly seen in BSE images of weathering rinds at the micron scale (Pope et al., 1995), as illustrated in **Figure 5**. One nanoscale hypothesis for this ubiquitous weathering-rind phenomenon of submicron fragments of iron oxide could be the ubiquitous presence of fungal hyphae.

Linking micrometer and nanoscales at the hand-sample level requires more than examination of just a few samples. However, pilot investigations of randomly selected samples do have the potential to suggest future research directions. A single sample from the Hawaii BSE study of olivine weathering (Wasklewicz et al., 1993; Wasklewicz, 1994) was reevaluated
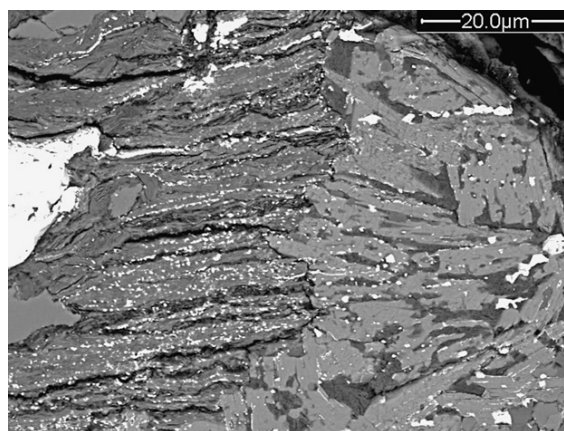

Figure 5 Cross section of the weathering rind of a metamorphic schist in the Phoenix Mountains, central Arizona. The bright mineral on the far left side is magnetite. Muscovite is the middle mineral, and hornblende is on the right side. Submicron clusters of iron oxides have precipitated throughout the muscovite and even into the hornblende. Iron mobilized from biotite has been observed to fracture rocks in Karkevagge (Dixon et al., 2002).

with HRTEM. This sample was collected from a Hualalai Volcano basalt flow f5d c8.2 ($\sim$2000 years old) and was covered with lichens. As in prior research (Bonneville et al., 2009), hypha appear to be able to exert enough pressure to split apart smectite clays in the weathering rind (**Figure 6(a)**).

As in prior research on bacteria weathering (Hiebert and Bennett, 1992), fungal hypha appear to be able to extract particular elements. Instead of potassium extracted from bioite
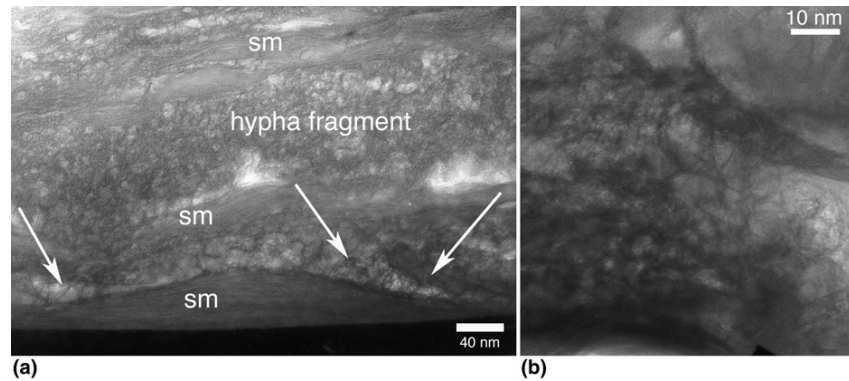
Figure 6 Fungal hyphae appear to be extracting calcium from olivine in the weathering rind of a Hualalai basalt flow covered by lichen. (a) Overview of the interface of a hypha (granular appearance), smectite clay (sm), and an olivine mineral (dark, thicker, and, hence, electron opaque at the bottom). Arrows show nanoscale strings of darker material that show a spike in calcium in energy dispersive measurements. Given that the lower end of typical hypha diameter is ∼2 μm, it is possible that this cross section shows an undulating hypha surface surrounded by smectite clay. (b) Close-up of the boundary between hyphae nanoscale strings of calcium and the underlying olivine (dark, thicker, and electron opaque at lower left).

(Bonneville et al., 2009), there is an uptake in calcium (**Figure 6**). EDS analyses reveal that there are strings in the imagery in **Figure 6**. These linear strings appear to be rich in calcium. The apparent source of the calcium appears to be an olivine grain. The reason for this uptake is uncertain. The calcium might be used in the formation of calcium oxalates produced by many lichen (Wadsten and Moberg, 1985; Bjelland and Thorseth, 2002) and fungi (Smits et al., 2009), or calcium might be used in another microbial process. Regardless of the need, nanoscale fungal weathering of olivine could provide yet one more explanation why Goldich's weathering sequence depends upon the presence of organisms and is incorrect where there exists minimal contact between minerals and biotic activity.

4.4.3.2 Crossing the Nanoscale to Micron-Scale Threshold

There is a danger involved in extrapolating nanoscale weathering observations to smaller scales. Misunderstanding of the threshold between processes operating at the micron scale and above versus the nanoscale environment can lead to confusion and misinterpretation. An example comes from the rock varnish literature where nanoscale instability was simply assumed to invalidate (Garvie et al., 2008, 2009) observations at the micron scale of over 10 000 microlamination sequences (see **Figure 7**) recording paleoclimatic fluctuations (Liu and Broecker, 2000; Liu et al., 2000; Zhou et al., 2000; Liu, 2003; Liu and Broecker, 2007, 2008a, 2008b; Liu, 2010). In summary, Garvie et al. (2008, 2009) analyzed three samples with HRTEM at the nanoscale, finding evidence for nanoscale instability of manganese oxides. They then made the scale jump to the micron scale and simply assumed that nanoscale instability meant that micron-scale paleoclimatic interpretations of over a decade rock varnish research by T. Liu and colleagues must be invalid (Dorn and Krinsley, 2011).

The issue here is not problems with the basic observation of nanoscale instability. Prior to Garvie et al. (2008, 2009), others noted that nanoscale instability of Mn-oxides is the key

to explaining how rock varnish forms (Potter, 1979; Dorn, 1998; Krinsley, 1998; McKeown and Post, 2001; Dorn, 2007). In one model of varnish formation, micron-scale microbial processes fix Mn and Fe oxides, followed by nanoscale instability that moves Mn and Fe oxides between bacterial casts and clay minerals. Ongoing shuffling of Mn–Fe oxides reoccurs at the nanoscale in the polygenetic model of varnish formation (**Figure 8**) (Krinsley, 1998; Dorn, 2007).

Thus, nanoscale instability is a key to varnish formation, but it does not invalidate micron-scale processes that lay down regular patterns at the micron scale. As Krinsley (1998: 721) explained:

> at the spatial scale of microns… some varnish appears quite stable with distinct layering patterns… At the spatial scale of nanometers as viewed with HRTEM, varnish appears to be in an open system… This is analogous to automobiles moving in a crowded parking lot, with oxides moving around until they find a suitable parking space in clay minerals.

Cars moving around inside a parking lot do not imply that the parking lot itself is unstable (Dorn and Krinsley, 2011).

The broader issue here is that the geochemistry of rock varnish instability at the nanoscale involves a great number of unknown issues. Every investigator who has explored varnish at the nanoscale agrees that Mn and Fe oxide instability is common (Krinsley et al., 1990, 1995; Dorn, 1998; Krinsley, 1998; McKeown and Post, 2001; Dorn, 2007; Garvie et al., 2008, 2009), but none of the HRTEM nanoscale observations infer that the extensively replicated micron-scale stratigraphy (Liu and Broecker, 2000; Liu et al., 2000; Zhou et al., 2000; Liu, 2003; Liu and Broecker, 2007, 2008a, 2008b; Liu, 2010) is invalid. This discussion highlights the danger of extrapolating nanoscale weathering observations to micron-scale phenomena.

In contrast to the above example of not recognizing a scale threshold, research that treats nanoscale processes as dramatically different can provide powerful explanations of weathering features. An example linking the soil profile scale
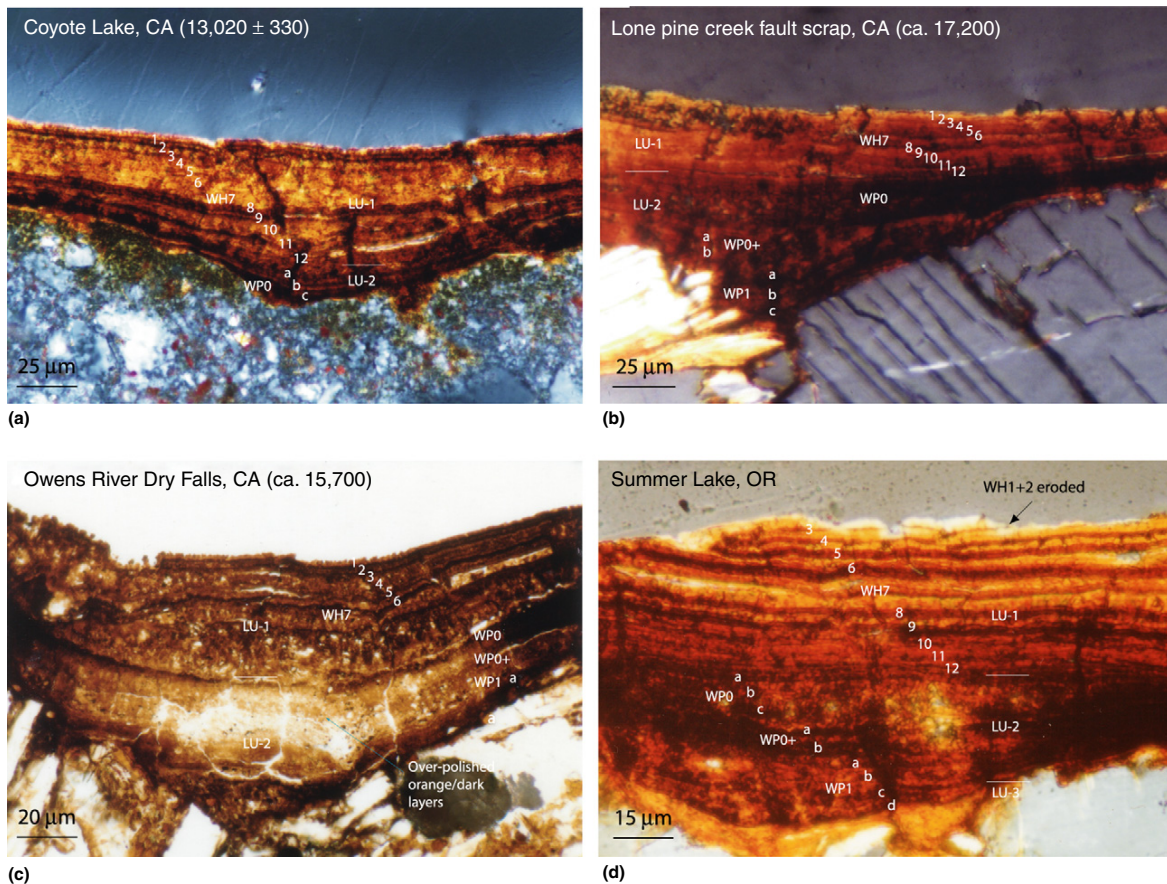
Figure 7 Microsedimentary basins with high rates of varnish accumulation show varnish microlaminations recording Holocene climatic changes. Black bands formed during wet periods in the Holocene termed WH (for wet Holocene) and multiple black bands in the terminal Pleistocene black layers WPO (Younger Dryas, wet Pleistocene black layer zero) and WP1 (wet Pleistocene black layer 1). Under the right conditions of fast accumulating varnish (images (c) and (d)) and proper thin section procedures, millennial and submillenial wet periods can be used successfully in geomorphic research (Liu and Broecker, 2008a). Although these varnishes started to form about the same time, faster accumulation rates for images (c) and (d) allow a higher resolution record than images (a) and (b). Images courtesy of T. Liu.

to the nanoscale is an investigation by Kaufhold et al. (2009) of an allophane unit in Ecuador that is about 20 000 ^{14}C years old and covers an area of over 4000 km^2. The unit is over 5 m thick and is up to 80% allophane by weight. In addition to documenting the geography and dimensions of the unit, this study analyzed the micrometer and nanometer scale aspects of the 15 nm scale allophane particles to inform on the volcanic and weathering formative settings of this unique deposit (Kaufhold et al., 2009). The large allophane deposit started with a particular volcanic eruption that was weathered *in situ* under an Andosol soil under conditions that developed a gradient of alkali earth metals sufficient to form the allophane.

4.4.3.3   Connecting Etching to Weathering Forms

Etching is a term used at almost all scales (**Figure 1**) in geomorphology, from etch plains that are erosion surfaces (Campbell and Twidale, 1991; Twidale, 2002), to etching that

generates karst weathering forms in sandstone (Young, 1988; Young and Young, 1992), to etching of minerals in soils used as a relative dating method (Locke, 1979, 1986), to nanoscale etch pits generated by bacteria and analyzed by atomic force microscopy (Buss et al., 2007). In the context of mineral weathering, however, analyses of etch pit morphologies are traditionally carried out with secondary electrons and sometimes backscattered electrons (Hall and Michaud, 1988; Lee and Parsons, 1995; White, 2005; Song et al., 2010), although they are sometimes studied at both the micrometer and nanometer scale (Hochella and Banfield, 1995; Brandt et al., 2003; Buss et al., 2007; Lee et al., 2007). As one would expect, isolated etch pits occur at the nanometer scale that "are typically only a few nanometers in depth and therefore not visible with SEM" (Brandt et al., 2003: 1457). Higher-resolution nanoscale research reveals that the nanotexture of minerals, produced by defects dislocation densities and patterns, plays a key role in how minerals weather (Banfield and Barker, 1994; Hochella and Banfield, 1995; Brown and Lee, 2007; Lee et al., 2007).
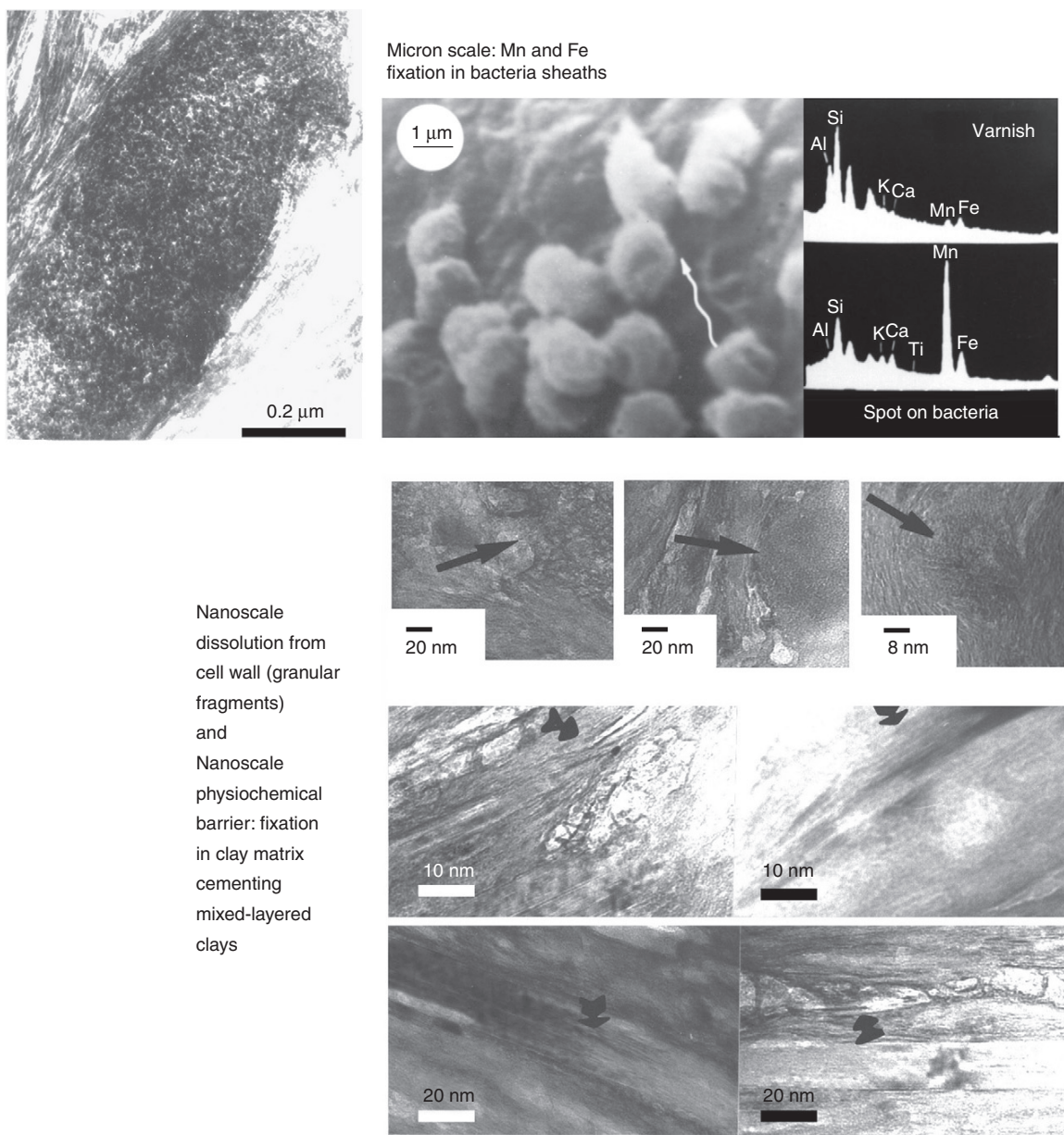
Micron scale: Mn and Fe
fixation in bacteria sheaths

1 µm

0.2 µm

Varnish

Si
Al
K Ca
Mn Fe

Mn
Si
Al
K Ca
Ti
Fe

Spot on bacteria

Nanoscale
dissolution from
cell wall (granular
fragments)
and
Nanoscale
physiochemical
barrier: fixation
in clay matrix
cementing
mixed-layered
clays

20 nm

20 nm

8 nm

10 nm

10 nm

20 nm

20 nm

Figure 8   Nanoscale instability of manganese and iron is a key to the formation of rock varnish. HRTEM and secondary electron microscopy images of cocci bacterial forms from Antarctic varnish and SEM/EDS reveals bacterial forms that concentrate manganese and iron at the micron scale. HRTEM of samples from Peru, Death Valley, and Antarctica illustrate nanoscale instability where oxides mobilize from bacterial sheath fragments, are transported a few nanometers, and then are fixed into mixed-layered illite-montmorillonite clays. These nanometer-scale Mn-oxides can be remobilized and refixed over and over again in a shifting nanoscale mineral structure (McKeown and Post, 2001: 712).

Studies of mineral etching at the nanoscale have raised a critically important conundrum with respect to clay mineral production by chemical weathering. Decades of thought about mineral weathering have generated a paradigm that feldspar chemical weathering always leads to clay mineral production, as supported by some of the first nanoscale weathering studies of feldspars (Banfield and Eggleton, 1990). More recent research, however, reveals that water-to-rock ratios in the weathering environment may be a key determinant in whether or not clay mineral alteration products occur at the nanometer scale (Lee et al., 2007). In other words, clay minerals do not always occur next to feldspar minerals; the nanoscale weathering environment is an important player, especially capillary scale and nanoscale water.

The scale jump connection between mineral nanoetching and much larger forms has not been considered in the literature, according to our understanding. Even linking hand-sample weathering forms and nanoetching has also not been

explored previously. However, we believe that making such a linkage is possible and propose here a speculative connection between nanoetching and the weathering form termed 'splintering' (Fitzner et al., 1997; Stoppato and Bini, 2003; Fitzner and Heinrichs, 2004; Dorn et al., 2008). Splintering is where all different types of rocks, from basalt to sandstone to schist to granite, have the appearance of pages of a book that has been wetted and then dried (Figure 9).

In the case of a foliated metamorphic rock, where grains are aligned, the weathering form of splintering is likely a consequence of differential weathering of more susceptible minerals at the micrometer to millimeter scale. Splintering simply reflects the millimeter to centimeter expression of micron-scale processes (Figure 10). However, splintering is a ubiquitous weathering form in virtually all rock types, even those with no obvious alignment of minerals. Explaining how this takes place at the hand-sample scale has not been a topic of focus in the geomorphic weathering literature.

A hypothesis that relates splintering forms (Figure 9) to the nanoscale alignment of etching is that subparallel alignment of mineral etching at the nanoscale can lead to alignment of capillary water conduits at the micrometer and then millimeter scales. These capillary water conduits appear to be key agents for the propagation of mineral weathering (Meunier et al., 2007).

Evidence in support of this hypothesis starts with a micrometer-scale image of feldspar weathering (Figure 11). From the perspective of Meunier et al. (2007), microfractures carry capillary water, and these fractures connect weathering pits recognized as initial porosity containing resident fluid. Microfractures propagate into the reaction area of these areas of initial porosity, just as streams propagate headward.

If splintering occurs when the enlarging microfractures (Meunier et al., 2007) encounter nanoscale etch features that are aligned, then the test of this hypothesis would be that splintering would not occur where nanoscale etching is not aligned. This appears to be the case, as evidenced by nanoscale lava weathering that does not display evidence of splintering (Figure 12).
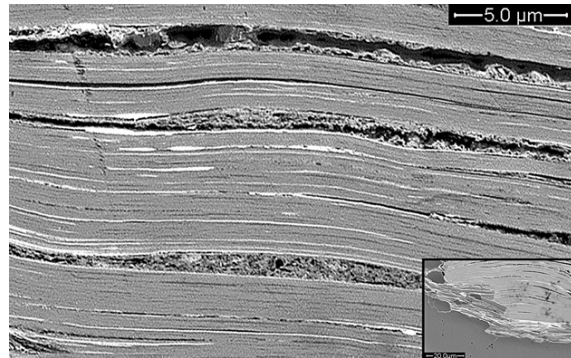

Figure 10 BSE image of biotite from a gneiss clast in a desert pavement near Florence, Arizona, undergoing a mix of splintering and grussification. The main aspect of this image feature is that the biotite itself has expanded volumetrically. Some of this expansion is due to the formation of secondary weathering products, such as the bright iron oxides or the darker material rich in silicon and aluminum. The inset image shows the broader context of biotite next to quartz, and how the biotite weathering breaks bonds between different minerals in the rock.
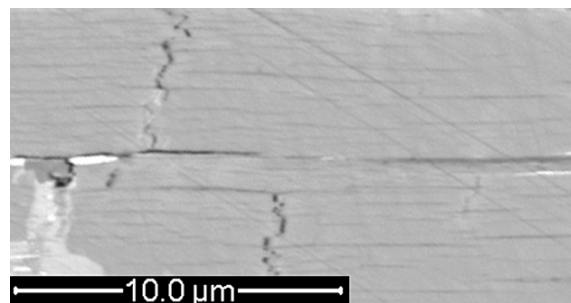

Figure 11 BSE image of a plagioclase in a hand sample showing splintering, Phoenix Mountains, Arizona. Horizontal parallel etching could relate to lattice imperfections, and there is also etching along perpendicular fractures. The diagonal marks are an artifact of sample polishing.

Figure 9 The weathering form of splintering seen at a hand-specimen scale (left, where the flower width is 2 cm) and where the talus boulder is 2 m tall (right). Left image is of hornfel at Black Canyon, Arizona; right image is of sandstone at Bryce National Park, Utah.
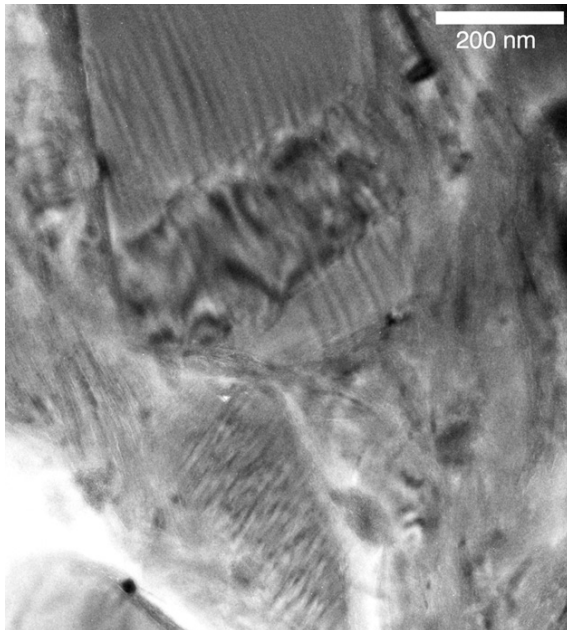
Figure 12 HRTEM image of plagioclase minerals illustrates etching at two scales. A finer scale of etching about 20 nm across could relate to lattice imperfections. This finer etching is perpendicular to a much larger etch feature that could relate to a larger mineral dislocation glide. The misalignment of etching patterns running in different directions could inhibit the growth of capillary water-bearing fractures in a subparallel alignment. The sample is from trachyandesite lava in the Akesu Volcanic field, Tibet (Wei et al., 2003). This sample shows no evidence of splintering.

Figure 13 presents a case study of a silicified dolomite from South Australia, where the alignment of splintering at the hand-sample scale corresponds with dissolution of microfractures carrying capillary water at the micron scale, and then also with alignment of connected weathered pores at the nanoscale. Nanoscale alignments appear to enable propagation of capillary water-bearing fractures in subparallel alignments that in turn generated the splintering weathering form seen at the hand-sample scale. By way of analogy, this conceptual model is similar to the way a parallel drainage pattern develops through taking advantage of fracture patterns.

4.4.3.4 Rock-Surface Alternation of Dust

Silt in the form of dust is ubiquitous on Earth (Goudie, 1978; Bullard and Livingston, 2009), Earth's moon (Gaier, 2005), Mars (Israel et al., 1997), and likely elsewhere. Weathering interactions within dust and between dust and underlying mineral surfaces are taking on increasing importance in understanding the decay of building stones (Sharma and Gupta, 1993; McAlister et al., 2006; Smith et al., 2007), formation of rock coatings on Earth (Dorn, 2009; Krinsley et al., 2009) and Mars (Johnson et al., 2002; Kraft et al., 2004), in understanding historic and prehistoric archaeology (Ganor et al., 2009), and in Quaternary research (Yaalon and Ganor, 1973; Kleber, 1997). Nanoscale research informs on dust production (Pye, 1987; Pye, 1989; Hochella, 2002a) and also
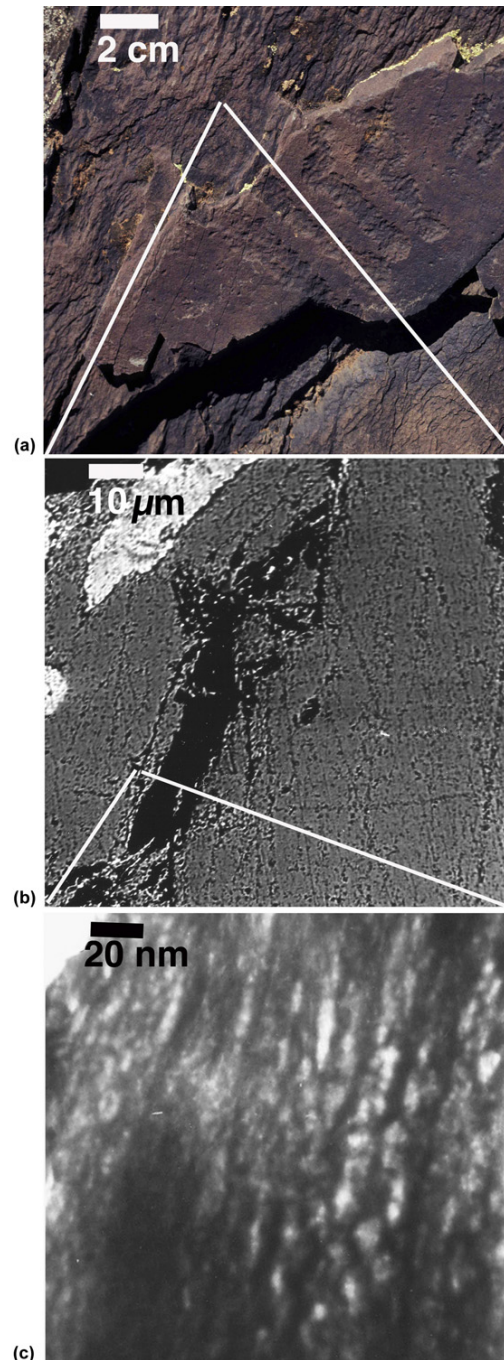

Figure 13 The weathering form of splintering of a silicified dolomite, South Australia ((a) – hand-sample scale), appears to correspond with the development of aligned micron-scale fractures that carry capillary water ((b) – micron-scale BSE image) and, in turn, with the alignment of nanoscale pores that are connected ((c) – nanoscale HRTEM image) and could be responsible for fostering the growth of micron-scale fractures. Locations of sample collection for analysis at progressively finer scales is indicated by the lines.
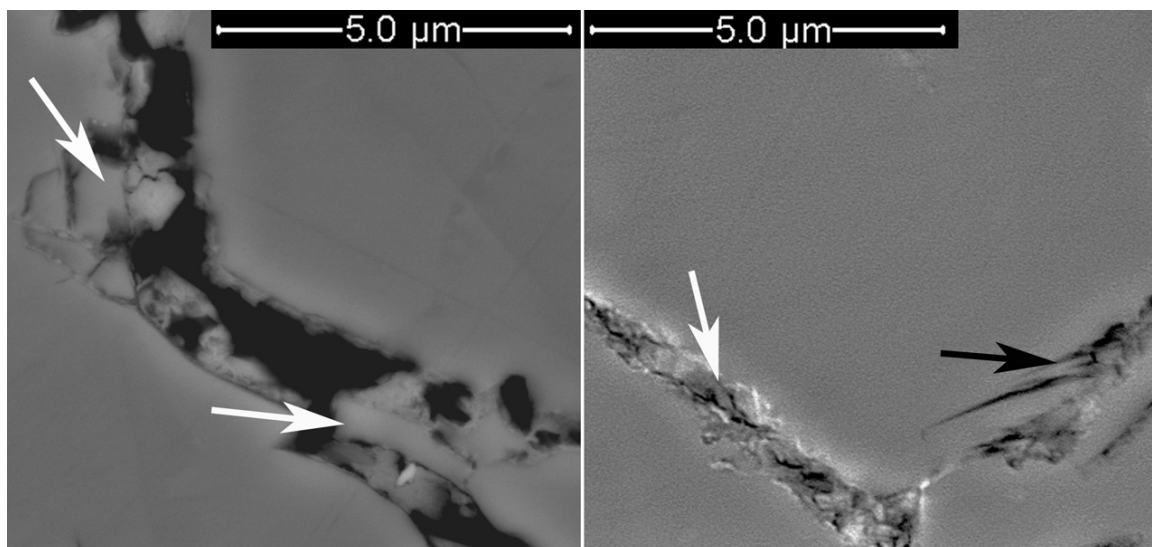
Figure 14   Images of quartz weathering observed in a desert pavement near Florence Junction, Arizona. These images show formation of silt-sized quartz fragments that appear to depend on both the existence of a fracture inside the quartz grain (white arrows) and also fragmenting along angles that are not aligned with the fracture (black arrows). For example, the subparallel fracturing seen in the right image likely relates to aligned crystal defects. However, the jigsaw puzzle appearance of quartz fragments on the edge of the fracture (upper left white arrow) in the left image is not easily explained by aligned defects.

what happens when dust deposits on rock surfaces as dust films and components of rock coatings.

Evidence exists that silt production is a function of inherent weaknesses in minerals such as quartz (Moss and Green, 1998; Smalley et al., 2005; Kumar et al., 2006), as well as external processes such as salt weathering, abrasion, frost weathering (Smalley and Krinsley, 1978; Whalley et al., 1982; Wright et al., 1998), microbial weathering of quartz surfaces (Brehm et al., 2005), and nanoscale interactions between quartz and water (Pope, 1995). The new generation of higher-resolution-BSE detectors is able to generate nanoscale resolution to illustrate both internal and external modes of quartz silt production (Figure 14).

The transition between wind-transported dust and dust as an integrated component of rock coatings has seen surprisingly little study. Even though there is a general consensus in the rock-coating literature that aeolian dust contributes to the formation of rock varnish, phosphate skins, and silica glaze (Potter and Rossman, 1977; Dorn, 1998, 2009; Langworthy et al., 2010), we do not know of a systematic study of nanoscale alternations of dust in the transition from rock-surface loess to rock-coating constituent.

We present here a nanoscale study of the transition from dust to rock coating in the Ashikule Basin, Tibet (Figure 15). The 4700–4800-m-high graben is a dusty, sulfate-rich, high-altitude, and high-ultraviolet (UV) flux environment. This field site offers the opportunity to study dust/substrate interactions distant from industrial pollution. The cold, dry, lower-air-pressure nature of the field suggests potential for a Mars analog site in part because the substrate is a lava flow, a trachyandesite of Ashishan Volcano in the Akesu Volcanic field (Wei et al., 2003).

While nanoscale mineral etching is of key importance as a process in chemical weathering, etched mineral surfaces could also play a role in the initial stages of the physical attachment of dust particles to mineral surfaces. Dust accretion on mineral surfaces is generally thought to occur from electrostatic or physical forces that hold dust particles together (Jordan, 1954; Bishop et al., 2002; Ganor et al., 2009). Nanoscale mineral etching creates an irregular surface that could play a key role in the initial attraction (Figure 16).

The particular sample selected for a detailed elemental nanoscale analysis is dust that accumulated on top of a rock coating that is a mixture of silica glaze and rock varnish. Silica glaze dominates this rock coating, but pods of rock varnish 2–40 μm across exist and are enveloped by the silica glaze (Krinsley et al., 2009; Langworthy et al., 2010). We selected a form with two oval shapes in the dust on top of the rock coating. This pod form has a texture suggestive of a biological origin (Figure 17), in that it has a granular texture similar to microbial hyphae observed elsewhere (Bonneville et al., 2009).

Our nanoscale investigation of grain alternation generated EDS data in a pattern of 300 points in a 10×30 matrix, where measurements are taken approximately 1.3 nm apart. Beam damage allows visualization (Lee, 2010) of the clear grid pattern (Figure 18). The grid serves as ground control points, allowing mapping of digital EDS data with geographic information system (GIS) software and subsequent visualization of nanoscale weathering.

Figure 19 displays a visualization of the 300-point grid of EDS data using a Kriging algorithm to map out elemental patterns. The dominant peaks in the EDS analyses consisted of the inorganic components of silicon and oxygen, and potential organic components of carbon and phosphorus. The highest concentrations of Si and O occur underneath the granular oval; this particle has a parallel structure suggestive of a clay mineral composition that would be consistent with the higher abundance of Si and O. By contrast, the highest
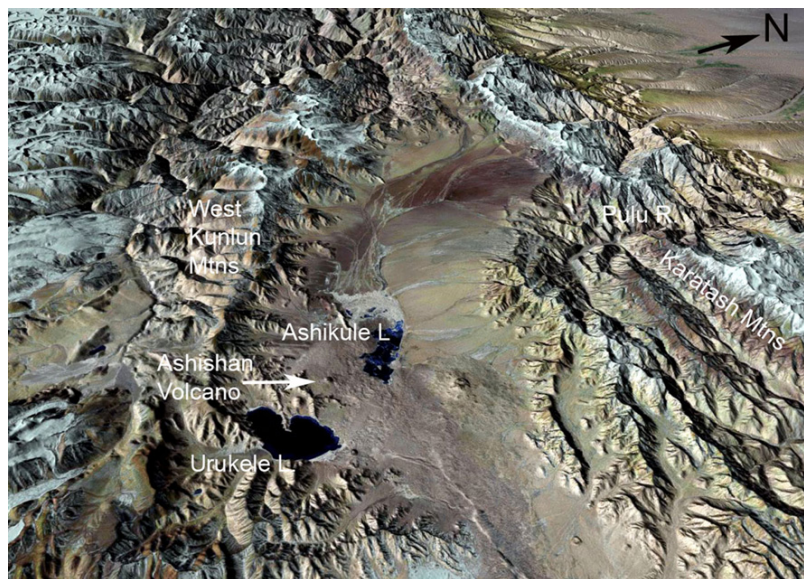
Figure 15 Ashishan Volcano study site in the Ashikule Basin, Tibet at 35.6988 N, 81.57623 E. The length of Urukele Lake is about 7 km, Ashikule Lake about 5.5 km, and the width of the graben at the location of the Ashishan Volcano is about 22 km. Modified from a raw image designed by William Bowen.
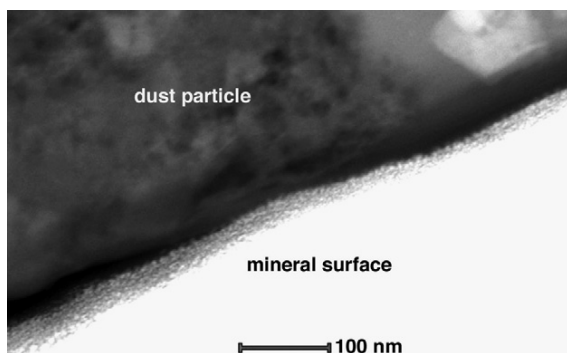

Figure 16 Mineral etching creates nanotopographic irregularities on the scale of less than 10 nm, as seen in this HRTEM image of cross section of a dust particle attracted to the underlying mineral surface of a rock. Nanoscale topographic irregularities likely contributed to the physical attachment of dust to this mineral surface, collected from the Akesu volcanic field, Tibet.

concentration of carbon occurs where the oval form displays a gray granular texture that transitions to an area of greater porosity with the lowest carbon concentrations. The area richest in C does appear to correspond with high P concentrations, but some areas of high P do have low concentrations of C. Banfield et al. (1999: 3407) found potential complex mixtures of clay minerals and complex organic polymers associated with microbial weathering, and this is possible for the analyzed oval in **Figures 18** and **19**.

Visualization of nanoscale spatial geochemistry with EDS grids has been accomplished in mineralogical research (Lee, 2010), but not analyzing rock coatings. Thus, the following interpretation of this single pilot analysis is speculative. Starting with the assumption that the oval particle had an organic origin, it appears as though Si and O (likely silica)
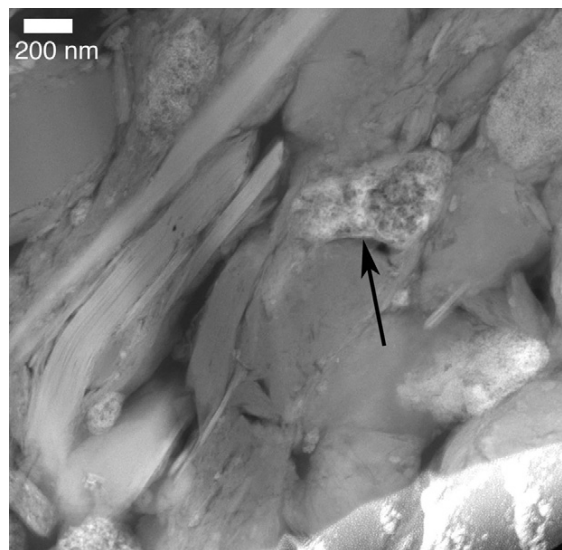

Figure 17 HRTEM image of dust particles on top of silica glaze and rock varnish. Many dust particles appear to be clay minerals, whereas others are fragments of other minerals. We selected a particle with two oval forms that could have a biotic origin (arrow). These oval forms appear to be undergoing post-depositional modification, as indicated by the uneven texture of bright and dark areas that suggest differential movement of elements.

have begun to migrate from the underlying clay inward – a possibility deduced by the gradient of Si and O from the clay at the bottom into the granular particle. The lower levels of C at the top of the grid could reflect the electron transparency of the middle of the oval form; picture sectioning a highly desiccated bacterial cell (or cross section of a desiccated fungal hypha). The thickest portions would be on the margins,

whereas the center would be thinnest – explaining why the lowest carbon concentrations occur in the middle of a possible desiccated microbial form. The behavior of phosphorus appears to link with a brighter area of the HRTEM image, and
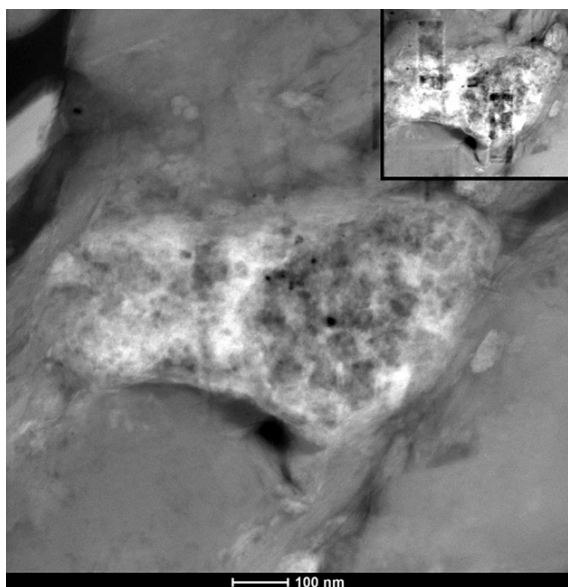

Figure 18   EDS data were collected in a grid pattern, where X-rays were generated every 1.3 nm apart. The center right part of the particle appears to be the most porous. The beam damage (seen in upper right inset image) creates a grid on the sample, and, thus, the precise locations of data are known and can be analyzed using geostatistical methods.

this bright area sends stringers toward the upper left. Like Si and O, the spatial pattern of phosphorus suggests nanoscale movement and hence instability. Our summary speculative interpretation of nanoscale instability is not unique to rock coatings such as rock varnish (Dorn, 1998; Krinsley, 1998; McKeown and Post, 2001) or silica glaze (Dorn, 1998; Gordon and Dorn, 2005b; Langworthy et al., 2010). However, it appears as though nanoscale movement of inorganic and possible organic components starts in dust deposits on rock surfaces – prior to envelopment inside a rock coating or incorporation into soils.

4.4.3.5   Silica Mobility in Rock Coatings and Case Hardening

Case hardening of the outermost shell of a rock commonly involves the migration of rock coating and other weathered products into pore spaces in the weathering rind of the rock (Conca and Rossman, 1982; Gordon and Dorn, 2005a; Dorn, 2009). Nanoscale studies into the processes by which this occurs in migration reveals new insights into how silica behaves on the surfaces of rocks. The first nanoscale investigation of silica glaze formation revealed that silica precipitates in the form of spheroids with diameters between 20 and 70 nm (Langworthy et al., 2010) as seen in **Figure 20**. EDS analyses by Langworthy et al. (2010) indicate that these spheroids are composed of just Si and O.

The spheroid diameters revealed by HRTEM are particularly significant for interpreting the behavior of water at the nanoscale. There is a transition between complete and partial wetting on silica surfaces between 20 and 70 nm (Zorin et al., 1992; Churaev, 2003). This is the size range of the observed

Figure 19   Nanoscale EDS mapping of a 300-point grid. Each grid point is approximately 1.3 nm apart, and the grid is 10 columns and 30 rows. The visual grid corresponds in size with maps of the four most common elements. **Figure 18** shows the larger context and a HRTEM pre-beam-damaged image of the analyzed area. The Kriging algorithm used to map out elemental patterns presents an intuitive color scale where lowest values are dark green and highest values are brown to pink.

Figure 20 HRTEM imagery of silica spheroids that have precipitated inside a pore space in the weathering rind (left). The silica spheroids composed of Si and O (Langworthy et al., 2010) are between 20 and 70 nm in diameter (right). Bright spots are artifacts.
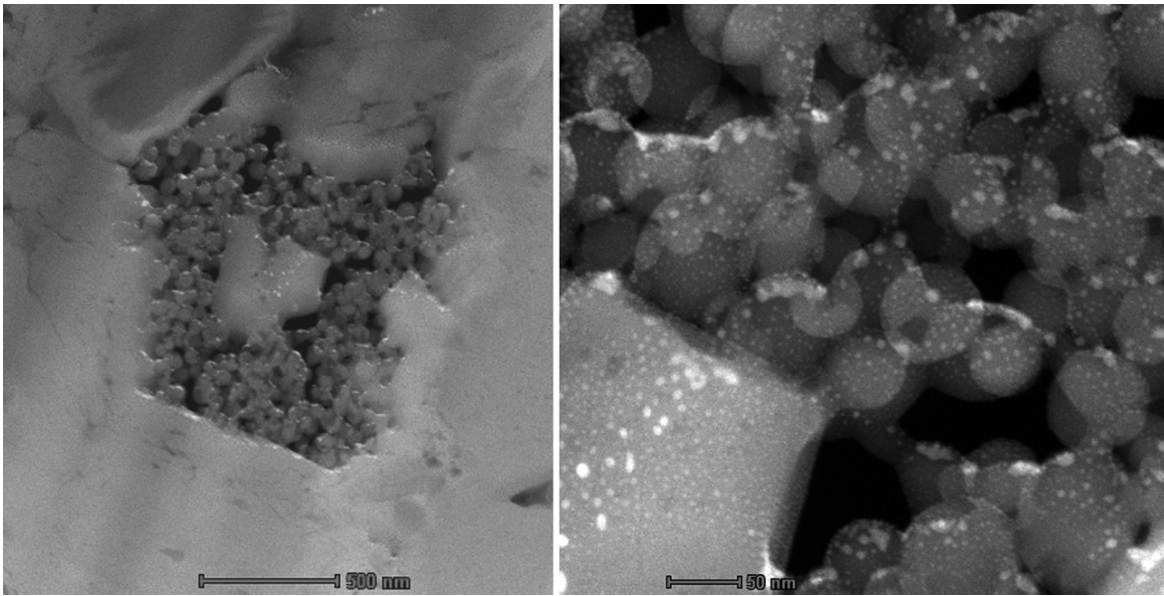
spheroids. Dorn (1998) originally suggested that crossing this transition ruptures the metastable wetting film (Zorin et al., 1992) resulting in silica precipitation – a hypothesis that is consistent with the presence of these spheroids (Langworthy et al., 2010).

Silica is an important case-hardening agent (Wilhelmy, 1964; Washburn, 1969; Conca and Rossman, 1982; Robinson and Williams, 1992; Mottershead and Pye, 1994; Dorn, 2004; Tratebas et al., 2004; Gordon and Dorn, 2005a). If the postulated model of silica glaze formation by spheroid deposition is found to occur in locations other than Tibet (**Figure 20**), there is every reason to suspect that silica would continue to remobilize and reprecipitate at the nanoscale, filling in pore spaces. HRTEM imagery (Langworthy et al., 2010) shows that the contacts between spheroids appear fused (**Figure 20**).

Furthermore, there is every reason to believe that silica movement should shift silica from rock coatings into the underlying weathering rind, hence case hardening the outer shell of a rock surface. Thus, it is possible that silica fills in voids in the weathering rind by growing new spheroids into pore spaces, since droplets ''do not cling to a surface immediately after formation, but move somewhat before they attach to the [pre-existing] solid'' (Koopal et al., 1999: 24). Thus, nanoscale silica instability could explain silica-impregnation and subsequent case hardening of weathering rinds.

4.4.3.6 Thermal Stresses

Studies of thermal stress at the micron scale reveal the need for higher resolution imagery to refine understanding of weathering processes (Mahaney and Milner, 2011). There is an awareness that fractures from thermal stresses should exist at the nanoscale (Van der Giessen and Needleman, 2002; Hall, 2006a, 2006b). However, we are not aware of nanoscale observations of frost weathering, insolation weathering, or fire

weathering. Thus, we present here a few initial observations of nanoscale features that relate to physical weathering from fire weathering and perhaps frost weathering.

An April–May 2000 wildfire burned about 37.5 km^2 of the Sierra Ancha Mountains, Arizona. Sandstone and diorite boulders originally surveyed in 1989 were resurveyed after the spring fire, after the summer monsoon season, and then after the winter 2001 season (Dorn, 2003). The most extensive postfire erosion of sandstone boulders did not take place after summer rains, but after winter precipitation. **Figure 21** presents an electron microscope image of quartz and plagioclase, where winter detachment took place within the weathered porous regions of the feldspar.

The original interpretation (Dorn, 2003) was that dissolution of feldspar took place in the weathering rinds over thousands of years before the fire, where moisture held in these pores may have played a role in accelerating fire spalling (Allison and Goudie, 1994).

A subsequent HRTEM investigation of this same sample indicates textural evidence that the mineral grains were subject to shear stress prior to spalling. Experiments on shearing associated with confined freezing and melting show lateral movement at the nanoscale (Christenson, 2001). An examination of lower-resolution imagery reveals that the feldspar grains have a ground-out appearance (middle image of **Figure 21**), and HRTEM images at the erosional surface reveal lattice displacement tens of nanometers wide (lower image of **Figure 21**). Although not in the original interpretation (Dorn, 2003), this new evidence of shearing at the eroded surface suggests that frost weathering may have contributed to accelerated erosion rates during the winter.

A 2001 wildfire at Whoopup Canyon, Wyoming, spalled sandstone joint faces that host rock art panels. A comparison of prefire samples collected in 1991 and postfire samples collected in 2003 (Tratebas et al., 2004) reveals that the fire
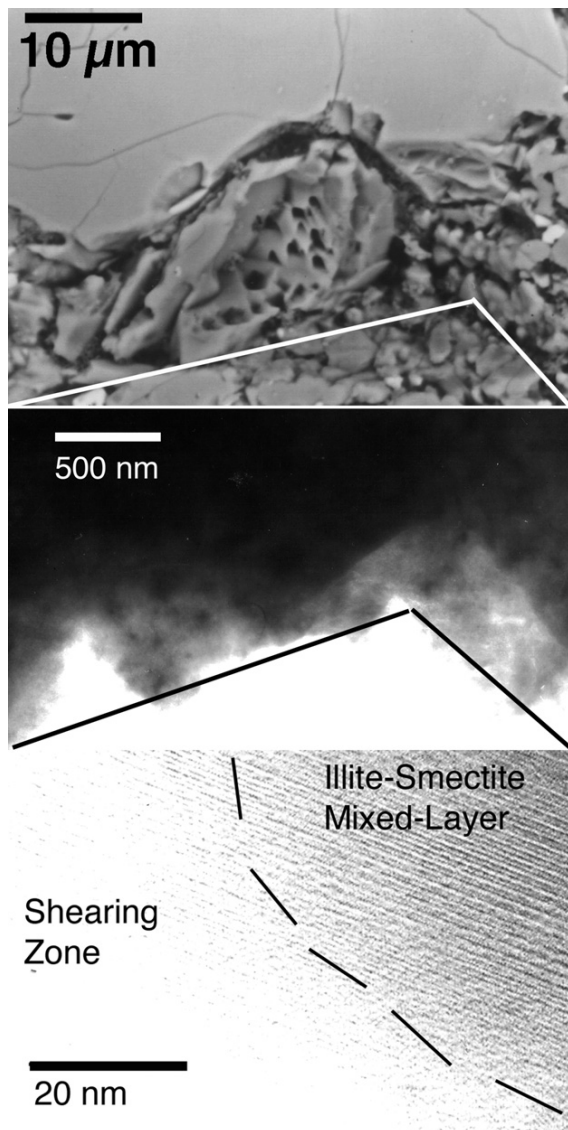
Figure 21 A spalled grain from sandstone Boulder 1.2 collected after the winter season in May 2001 from the Sierra Ancha Mountains, Arizona, after a wildfire (Dorn, 2003). The top image presents a scanning electron microscope view of quartz (less weathered upper part of the image) and plagioglase (lower porous weathered grain). The winter 2001 spall face cut across the heavily weathered plagioclase. The middle image of a lower resolution TEM view (location indicated by the telescoping lines) of the erosional surface presenting a chaotic mix of clays and less weathered feldspar fragments. The appearance appears jumbled and not well ordered, consistent with a shearing event. The bottom HRTEM image provides a nanoscale view of the spalled surface of an illite–smectite mixed-layer clay; disruptions would be consistent with shearing of the clay.

generated thermal fracturing in the quartz grains of the sandstone (**Figure 22**). A sample was extracted from a seemingly unfractured quartz fragment for HRTEM study; however, at the nanoscale the quartz was fractured into jagged pinnacles and other forms (**Figure 22**). Although light microscopy shows

a region of unfractured quartz appears just a little darker, a nanoscale view reveals jagged fracturing. We speculate that a detailed study of fire-shattered rock would reveal an array of twisted and distorted mineral fragments similar to this single sample.

One conclusion of micron-scale studies of fire weathering in the Sierra Ancha of Arizona (Dorn, 2003) and Whoopup Canyon in Wyoming (Tratebas et al., 2004) was that case hardening helps minimize erosion associated with fire weathering. Locations that did not undergo detachment from fire weathering at both study sites were rock surfaces where weathering-rind pore spaces had been infilled with silica (**Figure 23**), and this infilling of silica case hardened the weathering rind. At scales finer than the 20 μm diameter silica spheroids (**Figure 20**), before the transition between complete and partial wetting on silica surfaces (Zorin et al., 1992; Churaev, 2003), silica appears to be leached out of quartz in channels only a few nanometers wide (**Figure 23**). These silica flows into the pore spaces help cement grains together. Detachments after the fire took place underneath this case-hardened zone.

4.4.3.7 Silica Glaze Formation on Mars by Water Vapor Deposition

Nanoscale studies of rock coatings are certainly not limited to terrestrial samples. High-resolution STEM reveals the presence of iron-rich coatings on lunar samples. An iron-rich accretion less than 10 nm thick is chemically distinct from the underlying rock, perhaps vapor deposited (Noble and Keller, 2006). The planetary geology literature is replete with speculation on the occurrence of rock (or desert) varnish (Greeley, 1987; DiGregorio, 2002; Boston et al., 2008). However, a working hypothesis among some investigators is that coatings of silica glaze should be the most common rock coating on Mars (Dorn, 1998; Kraft and Greeley, 2000).

The pre-Noachian period of Mars is the period of accretion about four billion years ago. The Noachian period is represented by the oldest surfaces with the greatest density of impact craters and also with the greatest density of surfaces impacted by liquid water producing river valley networks. Silica glaze on Mars might relate to Noachian rainfall events (McSween et al., 1999).

An alternative is that silica glaze relates to liquid water films on mineral surfaces (Boynton et al., 2009) or perhaps water vapor interactions around springs (Allen and Oehler, 2008). Phoenix Landing Site research reveals that H_2O ice and vapor interacts with soil particles (Smith et al., 2009) and that water vapor concentrations can vary considerably (Whiteway et al., 2009). The presence of water vapor near and at the surface of Mars makes reasonable the hypothesis that billions of years of tiny amounts of water vapor interactions might play a role in generating accumulations of amorphous silica on Mars. This hypothesis was tested in a 20-year experiment (Dorn, 2012).

For 20 years, basalt rock chips were placed in a closed reaction vessel with circulating air containing 80% relative humidity. At no point did liquid water come into contact with basalt surfaces. Basalt rock chips that lacked any rock
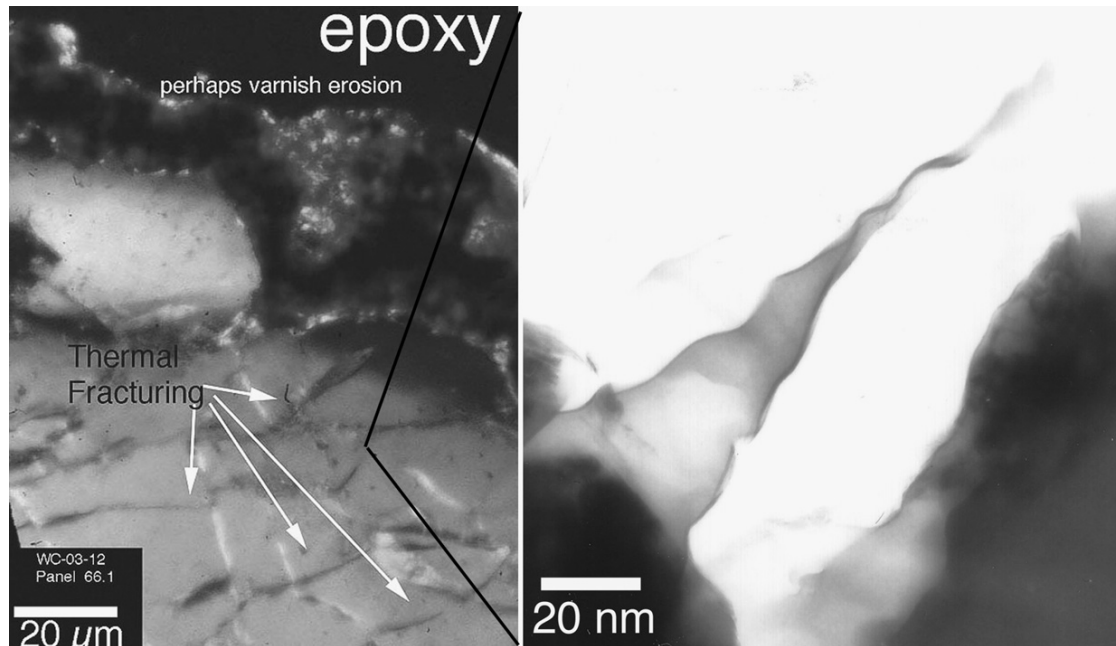
Figure 22 Sample WC-03-12 was collected from a sandstone joint face that acted like a fire chimney, resulting in fire erosion. The left image shows a light microscope thin section view of thermal fracturing in the quartz, exemplified by the arrows. Although fractures did occur in 1991 prefire samples, the abundance increased dramatically. The right HRTEM image reveals nanoscale fractures in segments of the quartz that appeared to be unfractured at the micrometer scale.

coatings at the start of the experiment had coatings of silica glaze formed entirely by water vapor by the end of the experiment. **Figure 24** shows the progressive accumulation of silica glaze on basalt chips removed from the reaction vessel after 5, 10, 15, and 20 years in response to only water vapor. The thickness appears to slowly increase in the first decade and then there is jump in thickness after 15 years of exposure to water vapor. By 20 years, the water-vapor-produced silica glaze was thick enough to image at the micron scale with BSE.

In addition to demonstrating that silica glaze could form without liquid water interactions, through nanoscale processes, this experiment also offers an explanation why silica glaze formation is favored over rock varnish and other rock coatings in humid environments like the rainshadows of Hawaiian volcanoes (Farr and Adams, 1984; Gordon and Dorn, 2005b); the abundance of humidity and the paucity of dust combines to favor silica glaze formation. The notion of nanoscape vapor deposition of rock coatings is not limited to Mars; space weathering has occurred on the surface of Itokawa through the accretion of a sulfur-bearing iron-rich 5 to 15 nm thick coating (Noguchi et al., 2011).

The source of the silica must have derived from the basalt chips. There is no other choice. Thus, there must be some nanoscale movement of silicon and oxygen from the underlying minerals toward the surface. Prior research on alpha–quartz reveals that hydration energies of water vapor absorption range from –90 to –28 kJ mol^{-1} (de Leeuw et al., 1999). Artificial silica powder samples are known to alter more under higher relative humidity (Morel et al., 2009). It is possible that silica–water vapor interactions occurred through

nanoparticle dissolution (Rimer et al., 2007) in the underlying mineral and then nanoparticle assembly on the surface (Rimer et al., 2008). The preliminary HRTEM observations (**Figure 24**), however, are insufficient to infer nanoscale processes. Still, the absence of a clear explanation of process does not deny the fundamental observation that silica glaze can accumulate on basalt mineral surfaces in just the presence of atmospheric water vapor.

While 80% is a relative humidity and a room temperature an absolute humidity far greater than found at the Mars-soil interface, this experiment reveals that liquid water is not needed to form coatings of silica glaze. Silica glaze could be forming on Mars now and over the billions of years where mineral surfaces have been exposed to water vapor near or on the surface of Mars.

4.4.3.8 Nanoscale View of Rock Polishing

This last case study explores something as simple as rock polishing. Those involved in weathering research regularly prepare cross sections and thin sections to examine samples in electron microscopes. Extremely smooth and well-polished surfaces are often a key for obtaining clear imagery using techniques such as BSE microscopy. Polishing is done in progressive stages of increasingly finer grits. Thus, from the perspective of sample preparation, polishing is a result of smoothing a surface.

However, micron-scale research on actively abraded surfaces described to have been polished is associated most typically with the presence of silica glazes in settings such as gibbers in Australia (Dorn, 1998: 282), abraded river cobbles
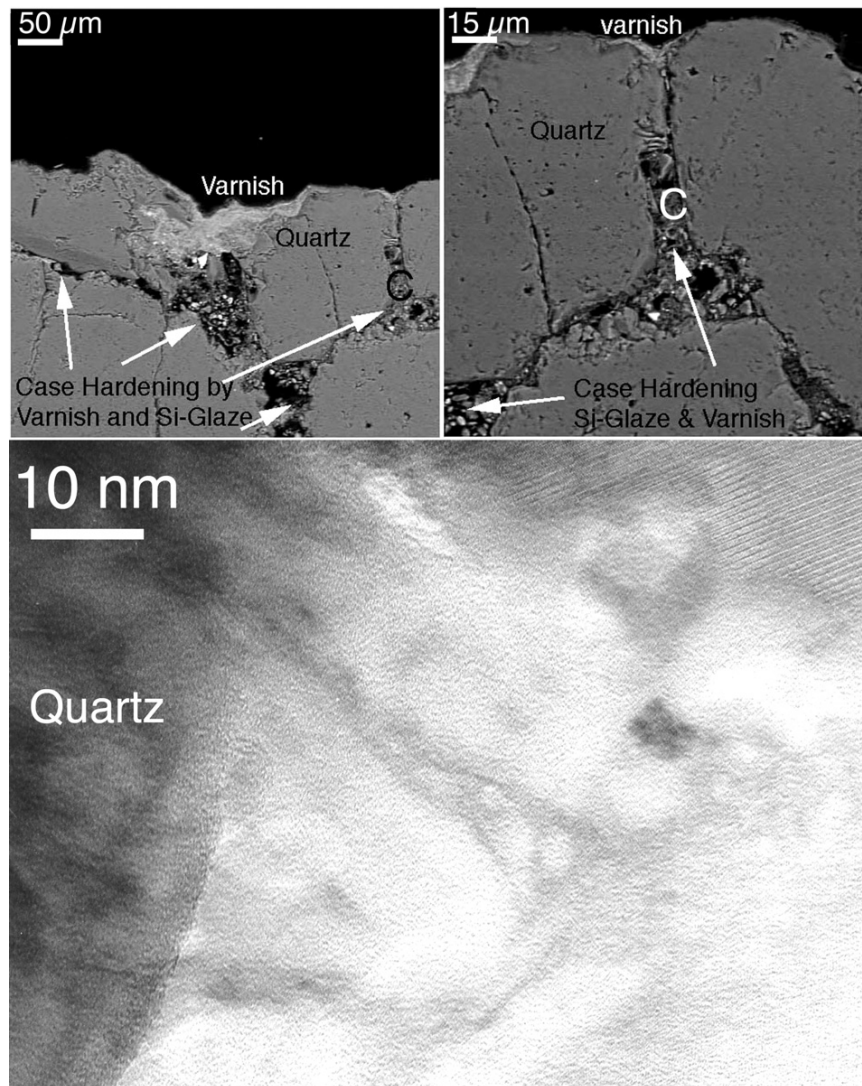
Figure 23   Samples collected from a Big Elk Petroglyph on Panel 6.2, collected from Whoopup Canyon, Wyoming (Tratebas et al., 2004), reveal how silica glaze infiltrates into the weathering rind. The three images were acquired at successively finer scales, where the letter C indicates the location of successive close-up imagery. The top two BSE images show the micron-scale context of how silica glaze infiltrates into pore spaces and cements sandstone quartz grains. The lower HRTEM image reveals what happens at the contact of the quartz grain and the pore space. The pore space has some clay minerals (e.g., upper right in lower HRTEM image), but much of the material at the quartz boundary appears to be amorphous. EDS analyses reveals that the silica appears to be mobilized from the quartz and moves into this amorphous material in what appears to be darker channels that are only a few nanometers across. This material could be a precursor to the silica spheroids presented in **Figure 20**.

(Dorn, 1998: 292), and glacially polished rock in Nepal and Mexico (Dorn, 1998: 303). In other circumstances, iron films are associated with active glacial polishing (Dorn, 1998: 96, 162) or iron films together with silica glaze (Dorn, 1998: 343). Although rock coatings may be responsible for some of the polished appearance, nanoscape perspectives paint a different picture.

Figure 25 illustrates the role of weathering in creating a polish. By weathering, we mean physical abrasion that fragments the rock (physical weathering), detaches rock fragments, and then erodes those fragments. Consider a sample of

glacially polished plagioclase phenocryst collected next to the Khumbu Glacier, Nepal (Figure 25(a)). The polishing appears to derive from a very smooth surface, where the only irregularities are undulations on the scale of a couple of nanometers. The polishing, therefore, represents physical weathering by abrasion and then eroding plagioclase fragments.

Rock polishing can also occur from the combination of physical abrasion and the addition of external materials. A slickenside collected from near Badwater in Death Valley had a distinct shiny polish. The polishing appears to be an effect
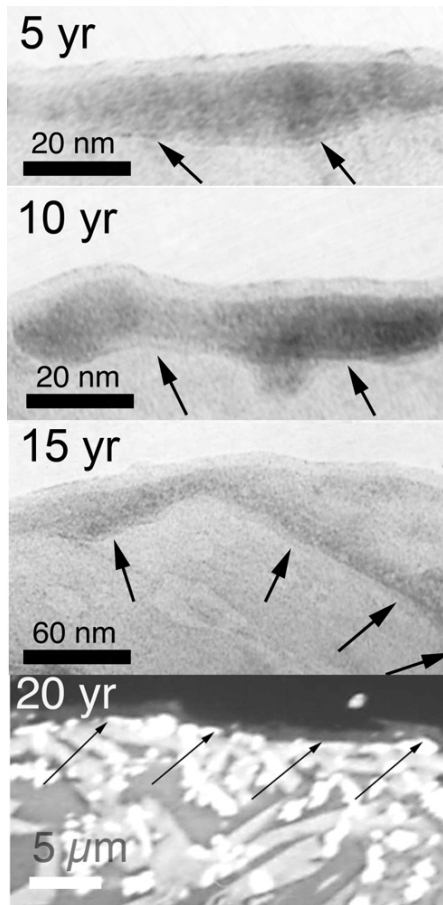
Figure 24 Silica glaze forms on basalt rock chips after exposure to only air with a relative humidity of 80% at 18 °C in a 20-year-long laboratory experiment. The label for each micrograph indicates how many years the basalt chip was exposed to the water vapor. Arrows point to the boundary between overlying silica glaze and the underlying mineral (plagioclase in for the three HRTEM images for years 5, 10, and 15). The very thin lighter band at the outer (upper) edge of each HRTEM image is an artifact of sample-beam interaction. The sample was not prepared in such a way that presence of spheroids could be imaged. In the case of the 20-year-BSE image, arrows show the contact between the darker (lower Z) silica glaze and the brighter (higher Z) underlying basalt minerals.

created by smearing of thin clay coating that is predominantly smectite mineralogy, similar to nanocoatings occurring along the San Andreas Fault (Schleicher et al., 2010) and in experimental studies (Han et al., 2011). Fragments of plagioclase weathered from the host rock were embedded in the smeared smectite, suggesting that some clay mineral weathering had taken place along the fault surface. Ongoing movements mixed the plagioclase from the rock and the smectite.

This last case study of polishing is intended to whet the appetite of the reader. Collect samples polished by active geomorphic processes – coastal, fluvial, aeolian, or glacial. Examine the sample with nanoscale tools (Figure 1). Something as simple as rock polishing may turn out to be complex and fascinating.

4.4.4 Conclusion

Weathering is a multidisciplinary arena explored by geochemists, soil scientists, geomorphologists, hydrologists, civil and environmental engineers, archaeologists, planetary geologists, and others interested in the breakdown and decay of rocks. Geomorphologists were among the first to explore the importance of nanoscale processes in weathering (Eggleton, 1980; Krinsley et al., 1995; Pope, 1995), even though nanoscale research in weathering has been dominated by geochemists over the past two decades (Banfield and Eggleton, 1988; Banfield et al., 1999; Hochella, 2002a; Waychunas et al., 2005; Hochella et al., 2008). A consequence of a general lack of attention to the nanoscale by geomorphologists has resulted in a situation where few connections exist between Earth's landforms and the nanoscale.

Certainly, weathering theory in geomorphology is concerned with scale (Pope et al., 1995; Phillips, 2000; Viles, 2001; Turkington et al., 2005; Hall, 2006b). However, the microscale in geomorphic weathering theory has been the subject of research at micrometer and higher scales. Nanoscale processes operating between 1 nm $(10^{-9}\,m)$ and 100 nm $(10^{-7}\,m)$ or 0.1 μm (Figure 1) do not reflect microscale conditions or processes.

Physical, electrical, magnetic, thermal, and kinetic properties differ dramatically across the nano–micron threshold (Hochella, 2002b; Zhang et al., 2003). The behavior of water in microfractures supporting capillary flow at the micron scale (Dorn, 2003; Dixon and Thorn, 2005; Meunier et al., 2007) does not reflect the behavior of nanoscale water (Lower et al., 2001; Zhang et al., 2003; Wang et al., 2006; Kalinichev et al., 2007; Langworthy et al., 2010). An example comes from brucite, a magnesium hydroxide that is a common weathering product (Kalinichev et al., 2007). Kalinichev et al. (2007) modeled three well-defined layers with respect to the behavior of water within 15 Å of a brucite surface. There is an inner layer of a few angstroms that is highly structured and contains water molecules with a high atomic density coordinated to the brucite surface. There is a middle transition layer about 4 Å from the surface with a low atomic density, and the outer layer that becomes similar to bulk nanoscale water about 5–15 Å from the surface. A similar result comes from studies of how water adheres to mica (Xu et al., 2010), where the first and second 0.4 nm layers of water behave like ice and accumulate at surface defects, but thicker accumulations of water are liquidlike.

A large realm of considerable challenge in nanoscale weathering research rests in explaining weathering forms such as those displayed in Figure 26. A biotite grain that is undergoing splintering has split into subparallel fragments as a result of nanoscale weathering processes by water accumulating at surface defects. The next generation of weathering researchers will link nanoprocesses to micron-scale forms with technology such as coupled dual-beam FIB-EM (Table 1).

Linking the nano- and micron scales will involve exceptionally different and hard-to-predict behavior such as biologically generated particles. In many cases, nanobiominerals are more stable (Tang et al., 2004) than would be expected of inorganic counterparts. In other cases, they are less stable (Dorn, 1998; Krinsley, 1998) than inorganic
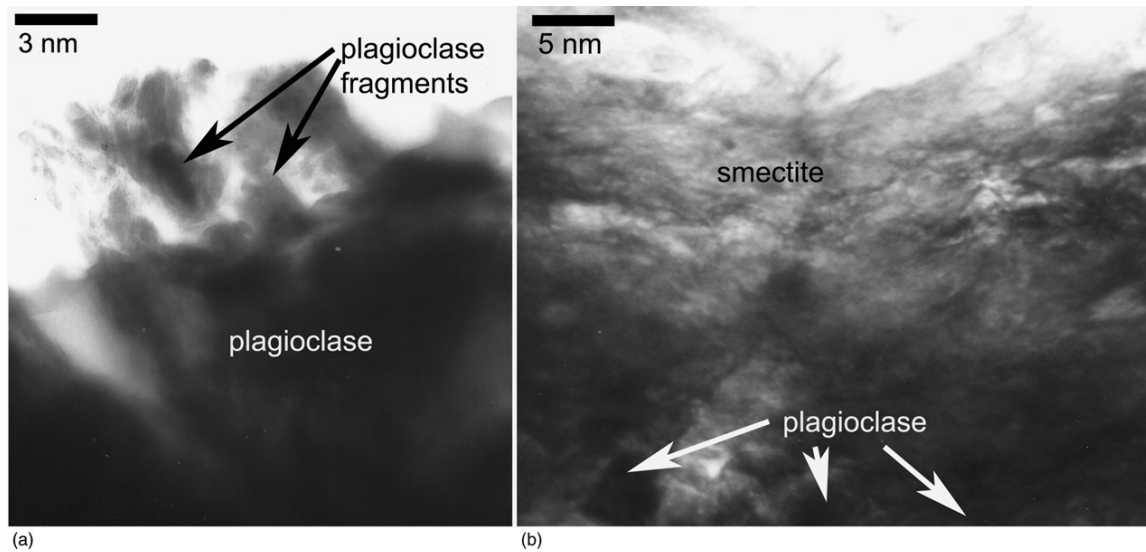
Figure 25 Lattice fringe HRTEM nanoscale imagery of geomorphologically abraded surfaces that display a polish in hand samples. Image (a) is a cross section of a glacially polished surface of a plagioclase phenocryst collected from the terminus of the Khumbu Glacier, Nepal. Image (b) is a cross section of polishing on a slickenside collected from an unnamed fault inside the Black Mountains near Badwater, Death Valley, California.
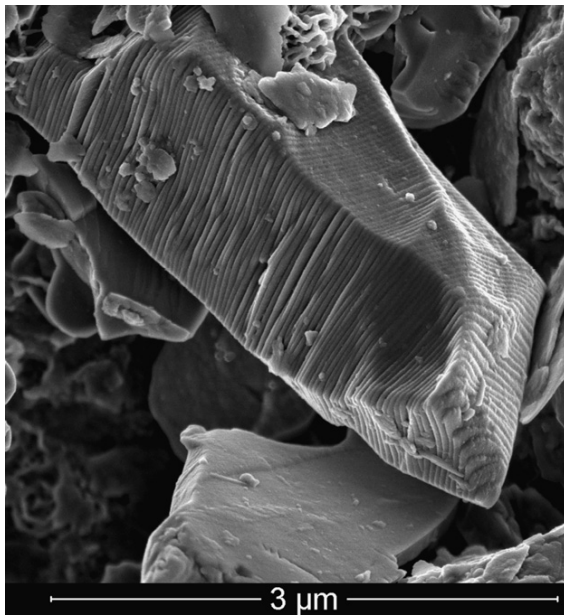

Figure 26 Weathering of biotite mineral, Adirondack Mountains, New York. The subparallel fracturing called splintering is a result of weathering that is taking place at the nanoscale.

counterparts, for reasons. Given the dominance of microorganisms on Earth (Reith, 2011), biologically generated particles will be a persistent issue in all aspects of nanoscale weathering.

Further development of weathering theory as it applies to understanding weathering forms needs to cross the nano–micron threshold. Unfortunately, very little research exists connecting nanoscale processes and geomorphic

weathering forms. For example, Hall (2006a: 388) argued that "little or no recognition has been given to either the processes or the measuring of attributes influencing the [freeze–thaw] processes or the measuring of attributes influencing the weathering processes, at the micro-scale, let alone the nano-scale." Until nanoscale observations are woven into the fabric of understanding basic processes such as frost weathering, it would be premature to develop geomorphic weathering theory further. We do not believe that there exists a sufficient understanding to be able to link the nano–micron threshold with a new theoretical understanding of landforms. Instead, this chapter represents an attempt to provide empirical case studies exemplifying why nanoscale matters to geomorphology.

We started by re-examining Goldich's (1938) classic weathering sequence, which argues that weathering is driven by the thermodynamics of mineral crystallization. In Goldich's sequence, olivine weathers first because it is most unstable in the low-temperature of Earth's surface. Although Goldich's sequence has been confirmed in humid study sites with an abundance of organisms and organic acid, some have found that olivine weathers last – not first – at locales that have experienced a minimum amount of organic activity (Wasklewicz et al., 1993; Wasklewicz, 1994). Support for a biotic explanation for olivine weathering, and hence the sequence of expected mineral instability has been found in studies of microorganisms (Barker, 1994; Barker and Banfield, 1996; Song et al., 2010). We present here additional nanoscale evidence for the importance of microbial processes through a study of the fungi in lichens where fungi uptake calcium from olivine in nanoscale veins (**Figure 6**). The broader geomorphic implication of invalidating Goldich's (1938) general sequence of mineral weathering rests in connecting mineral weathering sequences to landscape geochemistry (Perel'man, 1966; Fortescue, 1980) variability in the microscale and

nanoscale processes that appear to control the order of mineral weathering.

Nanoscale mineral etching could play a key role in determining weathering form at the hand-sample scale. An example comes from the splintering weathering form of parallel fracturing (Figure 9). Splintering occurs in all rock types, even those like basalt with millimeter-scale and micron-scale textures that do not appear to be well aligned with a subparallel orientation. One explanation, supported by a pilot study of splintered dolomite, is that nanoscale etching with a subparallel orientation allows micron-scale microfractures to extend with a subparallel geometry. These microfractures allow the movement of capillary water that then further develops these subparallel weaknesses into hand-scale splintered rock surfaces. We also propose that if nanoscale etching does not display a subparallel alignment, micron-scale microfractures do not propagate with a subparallel orientation and splintering does not occur.

Nanoscale processes are important in the geomorphic study of dust and dust deposition. Nanoscale defects are recognized as important in the production of silt (Smalley et al., 2005; Kumar et al., 2006), along with external weathering processes. Nanoscale topographic irregularities help dust adhere to mineral surfaces (Figure 16). We present here the first nanoscale mapping of geochemical alterations of a dust particle, probably biologically generated, adhered to a rock coating. Using a grid of 300 points 1.4 nm apart, we used EDS to map Si, O, C, and P. Silicon and oxygen appear to be migrating into the bioparticle from an external silicate, while phosphorus appears to be mobilizing from the outer to the inner portions of the particle (Figure 19). If we are correct that the particle has a biological origin, these findings present evidence for ongoing instability of biomineral deposits even as dust particles adhered to rock coatings.

Nanoscale processes help explain case hardening, an important reason why many rock surfaces remain stable – even as the internal portions of a weathered rock erode away (Washburn, 1969; Conca and Rossman, 1982; Dorn, 2004). Case hardening occurs where the porosity in the weathering rind has been filled in with material, typically mobilized from the overlying rock coating (Dorn, 1998; Gordon and Dorn, 2005a; Dorn, 2009). Silica is probably the most common and hence most important agent of case hardening. The first nanoscale study of silica glaze reveals that silica precipitates as 20–70 nm diameter spheroids, perhaps in response to crossing a transition between partial and complete wetting that occurs between 20 and 70 nm (Zorin et al., 1992; Churaev, 2003). One implication of these findings is that this silica is quite mobile, moving from surficial deposits of silica glaze down into pores in the underlying weathering rind (Figure 20).

This chapter is necessarily filled with speculation, trying to connect a few observations using HRTEM to research problems in weathering geomorphology. For example, a logical speculation is that the silica in the weathering rind could then be remobilized out of the weathering rind where core softening results in a cavern. Cavernous weathering forms typically have an outer shell of case-hardened rock that erodes slower than the core-softened rock. Formation of tafoni, for example, provides a gradient for capillary water flow, and there is no reason why the silica precipitated in weathering-rind pores (Figures 20 and 23) would not then be remobilized again toward cavern side walls. Thus, the nanoscale mobility and deposition of silica could be important in rock-coating formation, case hardening, and then stabilization of the inside walls of a cavernous weathering feature. The reason why such issues remain speculative is because the general problem of explaining differential weathering has not been a concern of geochemists who have pioneered nanoscale weathering research, but of geomorphologists.

The last theme of this chapter is the danger and potential of crossing the nano–micron threshold. The danger is illustrated by the type of thinking illustrated by Garvie et al. (2008, 2009), who analyzed three samples of rock varnish and concluded that nanoscale instability invalidated all prior research connecting rock varnish microlaminations to climatic change – research not based on three samples, but based on observations of over 10 000 microlamination sequences (Liu and Broecker, 2000; Liu et al., 2000; Zhou et al., 2000; Liu, 2003; Liu and Broecker, 2007, 2008a, 2008b; Liu, 2010). Thinking that observations on three samples invalidate research based on three orders of magnitude, more samples could be considered a prime case of scientific hubris. However, there is nothing wrong scientifically with nanoscale data obtained and presented by Garvie et al. (2008, 2009). In fact, prior research not mentioned by Garvie et al. (2008, 2009) similarly found nanoscale instability of varnish constituents (Figure 8) and concluded that this instability was a key in rock varnish formation (Dorn, 1998; Krinsley, 1998; Dorn, 2007). Rather, the fundamental danger illustrated by Garvie et al. (2008, 2009) was in a false assumption that the micron-scale processes associated with rock varnish microlaminations are the same as the nanoscale processes. Nanoscale movement does occur within laterally consistent varnish microlaminations, but this shifting does not invalidate the consistency of climatically controlled pattern so extensively documented in the literature (Liu and Broecker, 2000; Liu et al., 2000; Zhou et al., 2000; Liu, 2003; Liu and Broecker, 2007, 2008a, 2008b; Liu, 2010).

Despite the danger of assuming that nanoscale processes operate at micron or higher scales, there is considerable potential in crossing the nano–micron threshold. The potential is illustrated in Figure 13, where it is possible to connect quantitative rates of dissolution from the nanoscale to the hand-sample scale, and in Figures 21 and 22 where thermal stresses from wildfires generate nanoscale erosion. BSE imagery at different scales has been successfully processed to measure long-term rates of dissolution from field hand samples (Dorn, 1995; Dorn and Brady, 1995; Brady et al., 1999; Gordon and Brady, 2002). Similar data could be collected from HRTEM imagery and from samples originally analyzed through BSE. Scaling up and down becomes an issue of sampling procedure and the basic mechanics of preparing micrographs for digital-image processing. The benefits of making such a connection across scales have implications for explaining discrepancies between field and laboratory findings and also in developing a far deeper understanding of connections between geomorphology and landscape geochemistry (Perel'man, 1966; Fortescue, 1980).
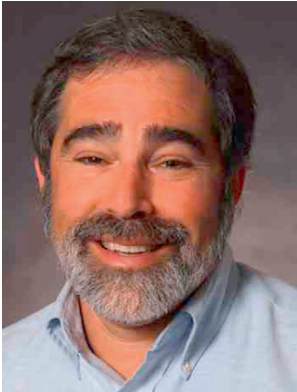
References

Allen, C.C., Oehler, D.Z., 2008. A case for ancient springs in Arabia Terra, Mars. Astrobiology 8, 1093–1112.

Allison, R.J., Goudie, A.S., 1994. The effects of fire on rock weathering: an experimental study. In: Robinson, D.A., Williams, R.B.G. (Eds.), Rock weathering and landform evolution. Wiley, Chichester, pp. 41–56.

Banfield, J.F., Barker, W.W., 1994. Direct observation of reactant–product interfaces formed in natural weathering of exsolved, defective amphibole to smectite: evidence for episodic, isovolumetric reactions involving structural inheritance. Geochimica Cosmochimica Acta 58, 1419–1429.

Banfield, J.F., Barker, W.W., Welch, S.A., Taunton, A., 1999. Biological impact on mineral dissolution: application of the lichen model to understanding mineral weathering in the rhizosphere. Proceedings National Academy of Sciences 96, 3404–3411.

Banfield, J.F., Eggleton, R.A., 1988. Transmission electron microscopy study of biotite weathering. Clays and Clay Minerals 36, 47–60.

Banfield, J.F., Eggleton, R.A., 1990. Analytical transmission electron microscope studies of plagioclase, muscovite and K-feldsapr weathering. Clay and Clay Minerals 38, 77–89.

Baram, M., Chatain, D., Kaplan, W.D., 2011. Nanometer-thick equilibrium films: the interface between thermodynamics and atomistics. Science 332, 206–209.

Barker, W.W., 1994. Biogeochemical weathering of hornblende syenite. EOS 74, 281.

Barker, W.W., Banfield, J.F., 1996. Biologically versus inorganically mediated weathering reactions: relationships between minerals and extracellular microbial polymers in lithobiontic communities. Chemical Geology 132, 55–69.

Bennett, P.C., Rogers, J.R., Choi, W.J., Hiebert, F.K., 2001. Silicates, silicate weathering, and microbial ecology. Geomicrobiology Journal 18, 3–19.

Benzerara, K., Menguy, N., Guyot, F., Vanni, C., Gillet, P., 2005a. TEM study of a silicate–carbonate–microbe interface prepared by focused ion beam milling. Geochimica Cosmochimica Acta 69, 1413–1422.

Benzerara, K., Yoon, T.H., Menguy, N., Tyliszczak, T., Brown, G.E., 2005b. Nanoscale environments associated with bioweathering of a Mg–Fe–pyroxene. Proceedings of the National Academy of Sciences 102, 979–982.

Bishop, J.L., Murchie, S.L., Pieters, C.M., Zent, A.P., 2002. A model for formation of dust, soil, and rock coatings on Mars: physical and chemical processes on the Martian surface. Journal of Geophysical Research 107(E11), http://dx.doi.org/10.1029/2001JE001581.

Bjelland, T., Thorseth, I.H., 2002. Comparative studies of the lichen–rock interface of four lichens in Vingen, western Norway. Chemical Geology 192, 81–98.

Bonneville, S., Smits, M.M., Brown, A., Harrington, J., Leake, J.R., Brydson, R., Benning, L.G., 2009. Plant-driven fungal weathering: early stages of mineral alteration at the nanometer scale. Geology 37, 615–618.

Boston, P.J., Spilde, M.N., Northup, D.E., Dichosa, A., 2008. Biogenic Fe/Mn oxides in caves and surface desert varnish: potential biosignatures for Earth and Mars. Astrobiology 8, 448.

Boynton, W.V., Ming, D.W., Kounaves, S.P., et al., 2009. Evidence for calcium carbonate at the Mars Phoenix Landing Site. Science 325, 61–64.

Brady, P.V., Dorn, R.I., Brazel, A.J., Clark, J., Moore, R.B., Glidewell, T., 1999. Direct measurement of the combined effects of lichen, rainfall, and temperature on silicate weathering. Geochimica et Cosmochimica Acta 63, 3293–3300.

Brandt, F., Bosbach, D., Krawczyk Bärsch, E., Arnold, T., Bernhard, G., 2003. Chlorite dissolution the acid pH-range: a combined microscopic and macroscopic approach. Geochimica Cosmochimica Acta 7, 1451–1462.

Brantley, S.L., 2005. Reaction kinetics of primary rock-forming minerals under ambient conditions. In: Drever, J.I. (Ed.), Surface and ground water, weathering, and soils. Treastise on Geochemistry. Elsevier, Amsterdam, vol. 5, pp. 73–117.

Brantley, S.L., Mellott, N.P., 2000. Surface area and porosity of primary silicate minerals. American Mineralogist 85, 1767–1783.

Brantley, S.L., Velbel, M.A., 1993. Preface to special issue on geochemical kinetics of mineral–water reactions in the field and the laboratory. Chemical Geology 105, vii–ix.

Brehm, U., Gorbushina, A.A., Mottershead, D.N., 2005. The role of microorganisms and biofilms in the breakdown and dissolution of quartz and glass. Palaeogeography, Palaeoclimatology, Palaeoecology 219, 117–129.

Brown, D.J., Lee, M.R., 2007. From microscopic minerals to global climate change? Geology Today 23(5), 172–177.

Bullard, J.E., Livingston, I., 2009. Dust. In: Parsons, A.J., Abrahams, A.D. (Eds.), Geomorphology of Desert Environments. Springer, New Work, NY, pp. 629–654.

Buss, H.L., Lüttge, A., Brantley, S.L., 2007. Etch pit formation on iron silicate surfaces during sideophore-promoted dissolution. Chemical Geology 240, 326–342.

Campbell, E.M., Twidale, C.R., 1991. The evolution of bornhardts in silicic volcanic rocks in the Gawler Ranges. Australian Journal of Earth Sciences 38, 79–93.

Casey, W.H., Banfield, J.F., Westrich, H.R., McLaughlin, L., 1993. What do dissolution experiments tell us about natural weathering? Chemical Geology 105, 1–15.

Christenson, H.K., 2001. Confinement effects on freezing and melting. Journal of Physics: Condensed Matter 13, R95–R133.

Churaev, N.V., 2003. Surface forces in wetting films. Advances in Colloid and Interface Science 103, 197–218.

Conca, J.L., Rossman, G.R., 1982. Case hardening of sandstone. Geology 10, 520–525.

DiGregorio, B.E., 2002. Rock varnish as a habitat for extant life on Mars. In: Hoover, R.B., Levin, G.V., Paepe, R.R., Rozanov, A.Y. (Eds.), Instruments, Methods, and Missions for Astrobiology IV. NASA, SPIE, Washington, DC, Vol. 4495, pp. 120–130.

Dixon, J.C., Thorn, C.E., 2005. Chemical weathering and landscape development in alpine environments. Geomorphology 67, 127–145.

Dixon, J.C., Thorn, C.E., Darmody, R.G., Campbell, S.W., 2002. Weathering rinds and rock coatings from an Arctic alpine environment, northern Scandinavia. Geological Society of America Bulletin 114, 226–238.

Dorn, R.I., 1995. Digital processing of back-scatter electron imagery: a microscopic approach to quantifying chemical weathering. Geological Society of America Bulletin 107, 725–741.

Dorn, R.I., 1998. Rock coatings. Elsevier, Amsterdam, 429 pp.

Dorn, R.I., 2003. Boulder weathering and erosion associated with a wildfire, Sierra Ancha Mountains, Arizona. Geomorphology 55, 155–171.

Dorn, R.I., 2004. Case hardening. In: Goudie, A.S. (Ed.), Encyclopedia of Geomorphology. Routledge, London, pp. 118–119.

Dorn, R.I., 2007. Rock varnish. In: Nash, D.J., McLaren, S.J. (Eds.), Geochemical Sediments and Landscapes. Blackwell, London, pp. 246–297.

Dorn, R.I., 2009. Desert rock coatings. In: Parsons, A.J., Abrahams, A. (Eds.), Geomorphology of desert environments. Springer, Amsterdam, pp. 153–186.

Dorn, R.I., 2012. Formation of silica glaze rock coatings through water vapor interactions. Physical Geography 33(1), 21–31.

Dorn, R.I., Brady, P.V., 1995. Rock-based measurement of temperature-dependent plagioclase weathering. Geochimica et Cosmochimica Acta 59, 2847–2852.

Dorn, R.I., Krinsley, D.H., 2011. Spatial, temporal and geographic considerations of the problem of rock varnish diagenesis. Geomorphology 130, 91–99.

Dorn, R.I., Whitley, D.S., Cerveny, N.C., Gordon, S.J., Allen, C., Gutbrod, E., 2008. The rock art stability index: a new strategy for maximizing the sustainability of rock art as a heritage resource. Heritage Management 1, 35–70.

Eggleton, R.A., 1980. High resolution electron microscopy of feldspar weathering. Clays and Clay Minerals 28, 173–178.

Emmanuel, S., Ague, J.J., 2011. Impact of nano-size weathering products on dissolution rates of primary minerals. Chemical Geology 282, 11–18.

Emmanuel, S., Ague, J.J., Walderhaug, O., 2010. Interfacial energy effects and the evolution of pore size distributions during quartz precipitation in sandstone. Geochimica et Cosmochimica Acta 74, 3539–3552.

Farr, T., Adams, J.B., 1984. Rock coatings in Hawaii. Geological Society of America Bulletin 95, 1077–1083.

Fitzner, B., Heinrichs, K., 2004. Photo atlas of weathering forms on stone monuments. http://www.stone.rwth-aachen.de/ (accessed June 2011).

Fitzner, B., Heinrichs, K., Kownatski, R., 1997. Weathering forms at natural stone monuments – classification, mapping and evaluation. International Journal for Restoration of Buildings and Monuments 3(2), 105–124.

Fortescue, J.A.C., 1980. Environmental geochemistry. A holistic approach. Springer, New York, NY, 347 pp.

Gaier, J.R., 2005. The Effects of Lunar Dust on EVA Systems during the Apollo Missions. NASA Center for Aerospace Information, Hanover, MD. NASA/TM—2005-213610.

Ganor, E., Kronfeld, J., Feldman, H.R., Rosenfeld, A., Ilani, S., 2009. Environmental dust: a tool to study the patina of ancient artifacts. Journal of Arid Environments 73, 1170–1176.

Garvie, L.A.J., Burt, D.M., Buseck, P.R., 2008. Nanometer-scale complexity, growth, and diagenesis in desert varnish. Geology 36, 215–218.

Garvie, L.A.J., Burt, D.M., Buseck, P.R., 2009. A microscopists view of desert varnish from the Sonoran Desert. Lunar and Planetary Science Conference 40, 1344.

Gleeson, D.B., Clipson, N., Melville, K., Gadd, G.M., McDermott, F.P., 2005. Characterization of fungal community structure on a weathered pegmatitic granite. Microbial Ecology 50, 360–368.

Gleeson, D.B., Kennedy, N.M., Clipson, N., Melville, K., Gadd, G.M., McDermott, F.P., 2006. Characterization of bacterial community structure on a weathered pegmatitic granite. Microbial Ecology 51, 526–534.

Goldich, S.S., 1938. A study of rock weathering. Journal of Geology 46, 17–58.

Gordon, S.J., Brady, P.V., 2002. *In situ* determination of long-term basaltic glass dissolution in the unsaturated zone. Chemical Geology 90, 115–124.

Gordon, S.J., Dorn, R.I., 2005a. *In situ* weathering rind erosion. Geomorphology 67, 97–113.

Gordon, S.J., Dorn, R.I., 2005b. Localized weathering: implications for theoretical and applied studies. Professional Geographer 57, 28–43.

Goudie, A.S., 1978. Dust storms and their geomorphological implications. Journal of Arid Environments 1, 291–310.

Greeley, R., 1987. Desert "varnish"; Earth, Mars, and Venus. International Union of Geodesy and Geophysics (IUGG), XIX general assembly; abstracts 1, 96.

Hall, K., 2006a. Monitoring of thermal conditions in building stone with particular reference to freeze–thaw events. In: Kourkoulis, S.K. (Ed.), Fracture and Failure of Natural Building Stones. Springer, Amsterdam, pp. 373–394.

Hall, K., 2006b. Perceptions of rock weathering in cold regions: a discussion on space and time attributes of scale. Géomorphologie: relief, processus, environnement 3, http://geomorphologie.revues.org/index146.html (accessed June 2011).

Hall, R.D., Michaud, D., 1988. The use of hornblende etching, clast weathering and soils to date alpine glacial and periglacial deposits: a study from southwestern Montana. Geological Society of America Bulletin 100, 458–467.

Han, R., Hirose, T., Shimamoto, T., Lee, Y., Ando, J., 2011. Granular nanoparticles lubricate faults during seismic slip. Geology 39, 599–602.

Hiebert, F.K., Bennett, P.C., 1992. Microbial control of silicate weathering in organic-rich ground water. Science 258, 278–281.

Hochella, M.F., 2002a. Nanoscience and technology: the next revolution in the Earth sciences. Earth and Planetary Science Letters 203, 593–605.

Hochella, M.F., 2002b. There's plenty of room at the bottom: nanoscience in geochemistry. Geochimica Cosmochimica Acta 66, 735–743.

Hochella, M.F., Banfield, J.F., 1995. Chemical weathering of silicates in nature: a microscopic perspective with theoretical considerations. In: White, A.F., Brantley, S.L. (Eds.), Chemical weathering rates of silicate minerals. Mineralogical Society of America, Washington, DC, pp. 353–406.

Hochella, M.F., Lower, S.K., Maurice, P.A., Penn, R.L., Sahai, N., Sparks, D.L., Twining, B.S., 2008. Nanominerals, mineral nanoparticles, and earth systems. Science 319, 1631–1635.

Israel, E.J., Arvidson, R.E., Wang, A., Pasteris, J.D., Jolliff, B.L., 1997. Laser Raman spectroscopy of varnished basalt and implications for in situ measurements of Martian rocks. Journal of Geophysical Research – Planets 102(E12), 28705–28716.

Johnson, J.R., Christensen, P.R., Lucey, P.G., 2002. Dust coatings on basaltic rocks and implications for thermal infrared spectroscopy of Mars. Journal of Geophysical Research – Planets 107(E6), Art No. 5035.

Jordan, D.W., 1954. The adhesion of dust particles. British Journal of Applied Physics 5, S194–S198.

Kalinichev, A.G., Wang, J., Kirkpatrick, R.J., 2007. Molecular dynamics modeling of the structure, dynamics and energetics of mineral–water interfaces: applications to cement materials. Cement and Concrete Research 37, 337–347.

Kaufhold, S., Kaufhold, A., John, R., et al., 2009. A new massive deposit of allophane raw material in Ecuador. Clays and Clay Minerals 57, 72–81.

Kleber, A., 1997. Cover-beds as soil parent materials in midlatitude regions. Catena 30, 197–213.

Koopal, L.K., Goloub, T., de Keizer, A., Sidorova, M.P., 1999. The effect of cationic surfactants on wetting, colloid stability and flotation of silica. Colloids and Surfaces A: Physicochemical and Engineering Aspects 151, 15–25.

Kraft, M.D., Greeley, R., 2000. Rock coatings and aeolian abrasion on Mars: application to the Pathfinder landing site. Journal of Geophysical Research – Planets 105(E6), 15107–15116.

Kraft, M.D., Michalski, J.R., Sharp, T.G., 2004. High-silica rock coatings: TES surface-type 2 and chemical weathering on Mars. Lunar and Planetary Science 35, 1936.

Krinsley, D., 1998. Models of rock varnish formation constrained by high resolution transmission electron microscopy. Sedimentology 45, 711–725.

Krinsley, D., Dorn, R.I., Anderson, S., 1990. Factors that may interfere with the dating of rock varnish. Physical Geography 11, 97–119.

Krinsley, D., Dorn, R.I., DiGregorio, B.E., 2009. Astrobiological implications of rock varnish in Tibet. Astrobiology 9, 551–562.

Krinsley, D.H., Dorn, R.I., Tovey, N.K., 1995. Nanometer-scale layering in rock varnish: implications for genesis and paleoenvironmental interpretation. Journal of Geology 103, 106–113.

Kumar, R., Jefferson, I.F., O'Hara-Dhand, K., Smalley, I.J., 2006. Controls on quartz silt formation by crystalline defects. Naturwissenschaften 93, 185–188.

Langworthy, K., Krinsley, D., Dorn, R.I., 2010. High resolution transmission electron microscopy evaluation of silica glaze reveals new textures. Earth Surface Processes and Landforms 35, 1615–1620.

Lee, M.R., 2010. Transmission electron microscopy (TEM) of Earth and planetary materials: a review. Mineralogical Magazine 74, 1–27.

Lee, M.R., Brown, D.J., Smith, C.L., Hodson, M.E., Mackenzie, M., Hellman, R., 2007. Characterization of mineral surfaces using FIB and TEM: a case study of naturally-weathered alkali feldspars. American Mineralogist 92, 1383–1394.

Lee, M.R., Parsons, I., 1995. Microtextural controls of weathering of perthitic alkali feldspars. Geochimica et Cosmochimica Acta 59, 4465–4488.

de Leeuw, N.H., Higgins, F.M., Parker, S.C., 1999. Modeling the surface structure and stability of a-quartz. Journal of Physical Chemistry B 103, 1270–1277.

Liu, T., 2003. Blind testing of rock varnish microstratigraphy as a chronometric indicator: results on late Quaternary lava flows in the Mojave Desert, California. Geomorphology 53, 209–234.

Liu, T., 2010. VML Dating Lab. http://www.vmldating.com/ (accessed June 2011).

Liu, T., Broecker, W.S., 2000. How fast does rock varnish grow? Geology 28, 183–186.

Liu, T., Broecker, W.S., 2007. Holocene rock varnish microstratigraphy and its chronometric application in drylands of western USA. Geomorphology 84, 1–21.

Liu, T., Broecker, W.S., 2008a. Rock varish evidence for latest Pleistocene millennial-scale wet events in the drylands of western United States. Geology 36, 403–406.

Liu, T., Broecker, W.S., 2008b. Rock varnish microlamination dating of late Quaternary geomorphic features in the drylands of the western USA. Geomorphology 93, 501–523.

Liu, T., Broecker, W.S., Bell, J.W., Mandeville, C., 2000. Terminal Pleistocene wet event recorded in rock varnish from the Las Vegas Valley, southern Nevada. Palaeogeography, Palaeoclimatology, Palaeoecology 161, 423–433.

Locke, W.W., 1979. Etching of Hornblende Grains in Arctic Soils: an indicator of relative age and paleoclimate. Quaternary Research 11, 197–212.

Locke, W.W., 1986. Rates of Hornblende Etching in Soils on Glacial Deposits. Baffin Island, Canada. Academic Press, New York, NY, pp. 129–145.

Lower, S.K., Hochella, M.F., Beveridge, T.J., 2001. Bacterial recognition of mineral surfaces: nanoscale interactions between Shewanella and alpha-FeOOH. Science 292, 1360–1363.

Mahaney, W.C., Milner, M.W., 2011. Lightning-induced changes in red pine (Pinus resinosa). Palaeogeography, Palaeoclimatology, Palaeoecology 309, 367–373.

McAlister, J.J., Smith, B.J., Torok, A., 2006. Element partitioning and potential mobility within surface dusts on buildings in a polluted urban environment, Budapest. Atmospheric Environment 40, 6780–6790.

McKeown, D.A., Post, J.E., 2001. Characterization of manganese oxide mineralogy in rock varnish and dendrites using X-ray absorption spectroscopy. American Mineralogist 86, 701–713.

McSween, Jr. H.Y., Murchie, S.L., Britt, D., et al., 1999. Chemical, multispectral, and textural constraints on the composition and origin of rocks at the Mars Pathfinder landing site. Journal of Geophysical Research 104(E4), 8679–8716.

Meunier, A., Sardini, P., Robinet, J.C., Pret, D., 2007. The petrography of weathering processes: facts and outlooks. Clay Minerals 42, 415–435.

Morel, B., Autissier, L., Autissier, D., Lemordant, D., Yrieix, B., Quenard, D., 2009. Pyrogenic silica ageing under humid atmosphere. Powder Technology 190, 225–229.

Moss, A.J., Green, P., 1998. Sand and silt graints: predetermination of their formation and properties by microfractures in quartz. Australian Journal of Earth Sciences 22, 485–495.

Mottershead, D.N., Pye, K., 1994. Tafoni on coastal slopes, South Devon, U.K. Earth Surface Processes and Landforms 19, 543–563.

Navarre-Sitchler, A., Brantley, S., 2007. Basalt weathering across scales. Earth and Planetary Science Letters 261, 321–334.

Noble, S.K., Keller, L.P., 2006. Investigating the nanoscale complexity of lunar space weathering. Geochimica Cosmochimica Acta Goldschmidt Conference Abstracts, A448. http://dx.doi.org/10.1016/j.gca.2006.06.900.

Noguchi, T., Nakamura, T., Kimura, M., et al., 2011. Incipient space weathering observed on the surface of Itokawa dust particles. Science 333, 1121–1125.

Paradise, T.R., 1995. Sandstone weathering thresholds in Petra, Jordan. Physical Geography 16, 205–222.

Perel'man, A.I., 1966. Landscape Geochemistry. Vysshaya Shkola, Moscow, 388 pp. (Translation No. 676, Geological Survey of Canada, 1972).

Phillips, J.D., 2000. Signatures of divergence and self-organization in soils and weathering profiles. Journal of Geology 108, 91–102.

Pope, G., Dorn, R.I., Dixon, J., 1995. A new conceptual model for understanding geographical variations in weathering. Annals of the Association of American Geographers 85, 38–64.

Pope, G.A., 1995. Newly discovered submicron-scale weathering in quartz: geographical implications. Professional Geographer 47, 375–387.

Pope, G.A., Meierding, T.C., Paradise, T.R., 2002. Geomorphology's role in the study of weathering of cultural stone. Geomorphology 47, 211–225.

Potter, R.M., 1979. The tetravalent manganese oxides: clarification of their structural variations and relationships and characterization of their occurrence in the terrestrial weathering environment as desert varnish and other manganese oxides. PhD Dissertation. California Institute of Technology, Pasadena.

Potter, R.M., Rossman, G.R., 1977. Desert varnish: the importance of clay minerals. Science 196, 1446–1448.

Pye, K., 1987. Aeolian Dust and Dust Deposits. Academic Press, London.

Pye, K., 1989. Processes of Fine Particle Formation. Dust Source Regions, and Climatic Change. Kluwer Academic Publishers, Dordrecht, 3–30.

Reith, F., 2011. Life in the deep subsurface. Geology 39, 287–288.

Rimer, J.D., Trofymluk, O., Lobo, R.F., Navrotsky, A., Vlachos, D.G., 2008. Thermodynamics of silica nanoparticle self-assembly in basic solution of monovalent cations. Journal of Physical Chemistry C 112, 14754–14761.

Rimer, J.D., Trofymluk, O., Navrotsky, A., Lobo, R.F., Vlachos, D.G., 2007. Kinetic and thermodynamic studies of silica nanoparticle dissolution. Chemistry of Materials 19, 4189–4197.

Robinson, D.A., Williams, R.B.G., 1992. Sandstone weathering in the High Atlas, Morocco. Zeitschrift fur Geomorphologie 36, 413–429.

Schiffbauer, J.D., Xiao, S., 2009. Novel application of focused ion beam electron microscopy (FIB-EM) in preparation and analysis of microfossil ultrastructures: a new view of complexity in early eukaryotic organisms. Palaios 24, 616–626.

Schleicher, A.M., van der Pluijm, B.A., Warr, L.N., 2010. Nano-coatings of clay and creep of the San Andreas Fault at Parkfield, California. Geology 38 (7), 667–670.

Sharma, R.K., Gupta, H.O., 1993. Dust pollution at the Taj Mahal – a case study. In: Thiel, M.-J. (Ed.), Conservation of Stone and Other Materials. E & FN Spon, London, pp. 11–18.

Smalley, I.J., Krinsley, D.H., 1978. Loess deposits associated with deserts. Catena 5, 53–66.

Smalley, I.J., Kumar, R., Dhand, K.O., Jefferson, I.F., Evans, R.D., 2005. The formation of silt material for terrestrial sediments: particularly loess and dust. Sedimentary Geology 179, 321–328.

Smith, B.J., McAlister, J.J., Baptista-Neto, J.A., Silva, M.A.M., 2007. Post-depositional modification of atmospheric dust on a granite building in central Rio de Janeiro: implications for surface induration and subsequent stone decay. Geological Society, London, Special Publications 271, 153–166,.

Smith, P.H., Tamppari, L.K., Arvidson, R.E., et al., 2009. H_2O at the Phoenix landing site. Science 325, 58–61.

Smits, M.M., Herrmann, A.M., Duane, M., Duckworth, O.W., Bonneville, S., Benning, L.G., Lundstrom, U., 2009. The fungal–mineral interface: challenges and considerations of micro-analytical developments. Fungal Biology Review 23, 122–131.

Song, W., Ogawa, N., Oguichi, C.T., Hatta, T., Matsukura, Y., 2010. Laboratory experiments on bacterial weathering of granite and its constituent minerals. Géomorphologie, Relief, Processus, Environnement 4, 327–336.

Stoppato, M.C., Bini, A., 2003. Deserts. Firely Books, Buffalo, 256 pp.

Swoboda-Colberg, N.G., Drever, J.I., 1993. Mineral dissolution rates in plot-scale field and laboratory experiments. Chemical Geology 105, 51–69.

Tang, R., Wang, L., Orme, C.A., Bonstein, T., Bush, P.J., Nancollas, G.H., 2004. Dissolution at the nanoscale: self-preservation of biominerals. Angewandte Chemie 43, 2697–2701.

Tratebas, A.M., Cerveny, N., Dorn, R.I., 2004. The effects of fire on rock art: microscopic evidence reveals the importance of weathering rinds. Physical Geography 25, 313–333.

Turkington, A.V., Paradise, T.R., 2005. Sandstone weathering: a century of research and innovation. Geomorphology 67, 229–253.

Turkington, A.V., Phillips, J.D., Campbell, S.W., 2005. Weathering and landscape evolution. Geomorphology 67, 1–6.

Twidale, C.R., 2002. The two-stage concept of landform and landscape development involving etching: origin, development and implications of an idea. Earth Science Reviews 57, 37–74.

Van der Giessen, E., Needleman, A., 2002. Micromechanics simulations of fracture. Annual Review of Material Research 32, 141–162.

Velbel, M.A., 1993. Constancy of silicate-mineral weathering-rate ratios between natural and experimental weathering: implications for hydrologic control of differences in absolute rates. Chemical Geology 105, 89–99.

Viles, H.A., 2001. Scale issues in weathering studies. Geomorphology 41, 61–72.

Wadsten, T., Moberg, R., 1985. Calcium oxalate hydrates on the surface of lichens. Lichenologist 17, 239–245.

Wang, J.Z., Kalinichev, A.G., Kirkpatrick, R.J., 2006. Effects of substrate structure and composition on the structure, dynamics, and energetics of water at mineral surfaces: a molecular dynamics modeling study. Geochimica Cosmochimica Acta 70, 562–582.

Washburn, A.L., 1969. Case hardening. In: Washburn, A.L. (Ed.), Weathering, Frost Action and Patterned Ground in the Mesters District, Northeast Greenland. Reitzels, Copenhagen, 15 pp.

Wasklewicz, T., 1994. Importance of environment on the order of mineral weathering in olivine basalts, Hawaii. Earth Surface Processes and Landforms 19, 715–735.

Wasklewicz, T., Dorn, R.I., Clark, S., et al., 1993. Olivine does not necessarily weather first. Journal of Tropical Geography 14, 72–80.

Waychunas, G.A., Kim, C.S., Banfield, J.F., 2005. Nanoparticle iron oxide minerals in soils and sediments: unique properties and contaminant scavenging mechanisms. Journal of Nanoparticle Research 7, 409–433.

Wei, H., Sparks, R.S.J., Liu, R., et al., 2003. Three active volcanoes in China and their hazards. Journal of Asian Earth Sciences 21, 515–526.

Whalley, W.B., Marshall, J.R., Smith, B.J., 1982. Origin of desert loess from some experimental observations. Nature 300, 433–435.

White, A.F., 2005. Natural Weathering Rates of Silicate Minerals. Elsevier, Amsterdam, pp. 133–168.

Whiteway, J.A., Komguem, L., Dickinson, C., et al., 2009. Mars water-ice clouds and precipitation. Science 325, 68–70.

Wilhelmy, H., 1964. Cavernous rock surfaces in semi-arid and arid climates. Pakistan Geographical Review 19(2), 8–13.

Wright, J., Smith, B., Whalley, W.B., 1998. Mechanisms of loess-sized quartz silt production and their relative effectiveness: laboratory simulations. Geomophology 23, 15–34.

Xu, K., Cao, P., Heath, J.R., 2010. Graphene visualizes the first water adlayers on mica at ambient conditions. Science 329, 1188–1191.

Yaalon, D.H., Ganor, E., 1973. The influence of dust on the soils during the Quaternary. Soil Science 116, 146–155.

Young, R., Young, A.R.M., 1992. Sandstone Landforms. Springer, Berlin.

Young, R.W., 1988. Quartz etching and sandstone karst: examples from the East Kimberleys, Northwestern Australia. Zeitschrift fur Geomorphologie 32, 409–423.

Zhang, H., Gilbert, B., Huang, F., Banfield, J.F., 2003. Water-driven structure transformation in nanoparticles at room temperature. Nature 424, 1025–1029.

Zhou, B.G., Liu, T., Zhang, Y.M., 2000. Rock varnish microlaminations from northern Tianshan, Xinjiang and their paleoclimatic implications. Chinese Science Bulletin 45, 372–376.

Zhu, C., Veblen, D.R., Blum, A.E., Chipera, S.J., 2006. Naturally weathered feldspar surfaces in the Navajo Sandstone aquifer, Black Mesa, Arizona: electron microscopic characterization. Geochimica Cosmochimica Acta 70, 4600–4616.

Zorin, Z.M., Churaev, N., Esipova, N., Sergeeva, I., Sobolev, V., Gasanov, E., 1992. Influence of cationic surfactant on the surface charge of silica and on the stability of aqueous wetting films. Journal of Colloid and Interface Science 152, 170–182.
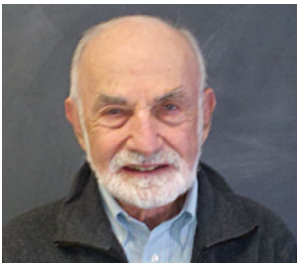
Biographical Sketch

Ronald I Dorn has been a professor of geography at Arizona State University, Tempe, Arizona since 1988. He served previously on the faculty at Texas Tech University. He is co-coordinator of the Arizona Geographic Alliance, a K-12 outreach program to promote geographic education in Arizona. He has been president and secretary/tresurer of the Geomorphology Specialty Group and as chair of the Nystrom Committee of the Association of American Geographers. He is a fellow of the Geological Society of America and the Arizona/Nevada Academy of Science, a Guggenheim Fellow, and a member of the Association of American Geographers and the American Rock Art Research Association.

Steven J Gordon is an associate professor of geosciences at the United States Air Force Academy. His specialties are geomorphology, spatial variations in rock weathering, and geographic information systems (GIS). Steve graduated from Arizona State University and has published extensively in the area of mineral weathering at the micron scale.

David Krinsley served in the Army during WWII. After that, he attended the University of Chicago where he received his PhD in geology. Following that, he took up a postdoctoral position at Columbia University. He then transferred to the Queens College, City University of New York, where he served as chairman of the Department of Geology, dean of sciences and acting provost (acting dean of the faculty). Four years were spent at the University of Cambridge, UK, where he was a visiting professor in the Department of Geology and an oversea fellow at Churchill College, University of Cambridge, UK. Leaving Queens College, he assumed the Chair at Arizona State University in Geology; upon retiring he moved to the Department of Geological Sciences at The University of Oregon, where he has been doing research in sedimentation and nanotechnology.

Kurt Langworthy is the director of nanofabrication and electron imaging at the Center for Advanced Materials Characterization in Oregon (CAMCOR). He has over 8 years of experience with transmission electron microscopy (TEM), scanning electron microscopy (SEM), and focused ion beam (FIB) instrumentation. Kurt graduated in 2006 from the University of Oregon where he achieved a masters degree in chemistry.